Nasir *et al.*
Low-carbon Materials and Green Construction (2025) 3:24
https://doi.org/10.1007/s44242-025-00084-8

Low-carbon Materials
and Green Construction

REVIEW

Open Access

Silicomanganese fume for sustainable construction: a recent review, ecological assessment, and future research roadmap

Muhammad Nasir[1], Ashraf A. Bahraq[2*], Rida Assaggaf[2], Shaik Inayath Basha[3] and Aziz Hasan Mahmood[4*]

Abstract

The lack of periodic safe disposal of silico-manganese wastes poses significant environmental and health risks. Producing each ton of silico-manganese alloy results in more than one ton of slag and 10%–15% fume, which can supplement cement in concrete. This study presents the first critical review of silicomanganese fume (SiMnF) for the synthesis of cementitious composites and evaluation of engineering properties. The review covers the fresh, hardened, and durability characteristics, along with the microstructural development of SiMnF-based Portland cement and alkali-activated products. It also examines the synergistic effects of SiMnF with other supplementary cementitious materials, focusing on rheological and mechanical aspects. The findings indicate that pre-treatment of raw materials and post-treatment of composites are essential for achieving target properties. Optimized dosage of SiMnF, alkaline activator concentration, and curing conditions can provide workable mixes with compressive strengths of up to 50 MPa. A detailed life-cycle assessment was conducted to quantify the environmental impact of SiMnF-based mixtures. Based on identified knowledge gaps, the study proposes a roadmap for future research. This review highlights the strategies for SiMnF from ferroalloy plants to be used in the cement and concrete industries, promoting solid waste management, reducing carbon footprints, and supporting sustainable development towards net-zero emission targets.

Keywords Waste management, Silicomanganese fume, Strength, Microstructure, Carbon footprint, Sustainability

摘要

硅锰废料若缺乏定期安全处置，会带来严重的环境和健康风险。每生产1吨硅锰合金，会产生超过1吨的炉渣和10%–15%的烟尘（硅锰烟，SiMnF），这些副产物可作为水泥替代材料用于混凝土。本研究首次系统综述硅锰烟在合成胶凝复合材料及其工程性能评价中的应用进展。该综述涵盖了基于硅锰烟的波特兰水泥和碱激发产品的新拌状态、硬化特性、耐久性以及微观结构演变过程。同时，研究了硅锰烟与其他辅助胶凝材料的协同效应，重点关注流变和力学性能。研究结果表明，原材料的预处理和复合材料的后处理是实现目标性能的关键。通过优化硅锰烟的掺量、碱激发剂浓度和养护条件，可以获得工作性良好的拌合物，其抗压强度可达50 MPa。研究还基于详细的全生命周期评估量化了硅锰烟基材料对环境的影响，并基于现有研究不足提出未来研究方向。此综述重点阐述了将硅锰烟从铁合金厂应用于水泥和混凝土行业的策略，从而促进固体废物管理、减少碳足迹，支持可持续发展，并助力净零排放目标的实现。

*Correspondence:
Ashraf A. Bahraq
ashraf.bahraq@kfupm.edu.sa
Aziz Hasan Mahmood
aziz.mahmood@uts.edu.au
Full list of author information is available at the end of the article

关键词 废物管理，硅锰烟尘，强度，微观结构，碳足迹，可持续性

1 Introduction

The largest synthetic compound and second-most widely consumed material on Earth is cement, following the indispensable consumption of water. The primary function of cement is to provide hydraulic binding properties to the concrete matrix. As a result of such attributes, the basic infrastructural needs of iconic buildings have been made practicable. It has been estimated that the current global demand for cement stands at 4.6 billion tons, with expectations for it to reach around 6 billion tons by 2050 [1]. This increase in cement production correlates with the growth of global population. The global construction boom presents a pressing concern due to the substantial energy demands of cement production and the carbon emissions from the calcination of limestone to produce cement. Approximately 70%–80% of the overall energy consumption in cement production occurs during the formation of clinker, accounting for 2% of global energy usage and 5% of industrial energy consumption [2]. Consequently, energy expenses represent a significant portion, ranging from 20% to 40% of total manufacturing costs [2, 3]. Addressing these challenges requires a shift towards more sustainable practices in cement usage to reduce consumption and offset demand for this carbon-intensive product. This includes substituting raw materials and fuel technologies, such as utilizing blended cements and adopting co-processing methods [4]. Furthermore, integrating supplementary cementitious materials (SCMs), such as waste and by-products, to substitute Portland cement (PC) either partially or entirely, stands out as a highly promising advancement for reducing emissions within the construction sector [5, 6].

Solid waste utilized in concrete mixes falls into three main categories: industrial or agricultural waste, municipal solid waste, and construction and demolition waste. Typically, these waste materials are either burned in the open air, sent to landfills, or stockpiled without recycling, particularly in developing countries. Open field burning is a cost-effective method used to improve the rotation of the crop cycle. However, it is associated with numerous environmental and health issues due to the release of fine particles and gases such as fine particulate matter, carbon monoxide, methane, polycyclic aromatic hydrocarbons, polychlorinated dibenzo-p-dioxins, polychlorinated dibenzofurans, elemental carbon, and organic carbon. These substances are light and can disperse in the air and cause acute respiratory effects and other health problems when inhaled unknowingly by people [7]. Similarly, industrial emissions often possess detrimental characteristics, such as toxicity, corrosiveness, flammability, chemical reactivity, and infectiousness [8]. Landfilling exacerbates space scarcity issues and poses risks of landslides. To mitigate these problems, several countries have implemented landfill taxation laws to reduce the volume of waste sent to landfills and to address issues like noise, odor, and pollution. These levies have continuously increased, varying based on waste type. For example, taxes on combustible waste surged from €15 to €50 per ton between 1993 to 1997, reaching €75 per ton by 2007, and increased by 50% as of July 2015 [9]. Additionally, landfilling can increase landslide risks, endangering human life and property.

Developing a robust solid waste management plan is essential to address environmental concerns and cost considerations effectively. A promising solution involves utilizing these solid wastes in infrastructural applications to promote green construction [10, 11]. These waste materials can serve as replacements for fine or coarse aggregates. In this regard, concrete technologists are increasingly exploring the incorporation of agricultural waste materials, such as oil palm, date palm, rice husk, sugarcane bagasse, wheat straw, coconut coir, corncob, elephant grass, bamboo, and olive waste, in concrete production [12]. Additionally, industrial byproducts from steel manufacturing, such as ground granulated blast furnace slag (GBFS), and from ferrosilicon production, like silica fume (SF), as well as residues from coal-powered power plants, such as fly ash (FA), have been widely utilized [13, 14]. Natural SCMs like red mud, metakaolin, calcined clay, and natural pozzolan are also gaining broad attention [15–19]. Despite these advancements, there is a constant need to identify additional potential waste products and enhance existing materials and technology. For instance, by-products from the ferroalloy industry, including silicomanganese slag (SiMnS) and silicomanganese fume (SiMnF), are relatively rare in the literature. These materials contain high concentrations of manganese oxide (MnO), potassium oxide (K_2O), and silica (SiO_2) [20, 21]. They present opportunities for value-added applications in construction products, either within the PC system or through alkali-activated/geopolymer technology [22–25].

In recent years, there has been a growing interest in assessing the potential of SiMnF as a sustainable construction material. Despite emerging studies, a comprehensive review of SiMnF-based mortar and concrete mixtures, their composition, performance, and practical relevance, has been lacking. Given the increasing global

generation of SiMnF, the urgent demand for low-carbon construction solutions, and the broader shift toward industrial by-product utilization, consolidating existing knowledge is both timely and necessary. This paper presents the first thorough review of SiMnF, analyzing various aspects of its production, application, properties, and implications. Initially, the paper addresses the challenges associated with manganese alloy production, including the ferroalloy production process and the concentration of manganese in the vicinity of such plants, emphasizing the health risks linked with manganese exposure (Sect. 2). The physical and chemical properties of SiMnF are presented (Sect. 3). It then explores the utilization of SiMnF waste in construction applications alongside the synthesis of SiMnF-based mixtures (Sect. 4). The review discusses the fresh and hardened properties of these mixtures, focusing on their rheological and mechanical aspects, and investigates their performance in normal and alkali-activated mortars (Sect. 5). The microstructural analysis, including scanning electron microscopy (SEM), energy dispersive X-ray spectroscopy (EDS), X-ray diffracation (XRD), Fourier transform infrared spectrometry (FTIR), and thermogravimetric analyses of SiMnF composites, is reviewed to provide insights into their microstructural characteristics (Sect. 6). Additionally, the review examines the durability properties (Sect. 7), conducts a sustainability assessment (Sect. 8), and identifies challenges and future perspectives (Sect. 9). Finally, summarized conclusions were highlighted (Sect. 10). In general, this state-of-the-art review of literature elucidates the insights on exploiting SiMnF from ferroalloy facilities in the cement and concrete sectors, advancing solid waste management, minimizing carbon emissions, and fostering green infrastructural development in pursuit of net-zero emission goals.

2 Manganese alloy production and associated problems

Manganese (Mn) is positioned as the 25th element on the periodic table, and it is recognized as the 12th most prevalent element in the Earth's crust, as well as the 4th naturally occurring metal [20]. According to the International Manganese Institute (IMnI), present global reserves of Mn, including low-grade ores, are estimated to be several billion tons. In 2011, the reserves of high-grade ores (with Mn content greater than 44%) reached 680 million tons. From these reserves, the production of Mn alloy was recorded to be 17.7 million metric tons (MMT). According to the 2009 statistics, the countries with the highest Mn reserves and production (in MMT) were: Ukraine (140 reserves and 0.31 production), South Africa (130 reserves and 1.3 production), Australia (87 reserves and 1.6 production), India (56 reserves and 0.96 production), Gabon (52 reserves and 0.81 production), China (40 reserves and 2.4 production), Brazil (29 reserves and 0.99 production). The remaining countries have a negligible Mn reserve and a production of 1.2 MMT, as shown in Fig. 1. Approximately 93% of global Mn alloy production is primarily used in the production of steel, as there is no suitable alternative for Mn in this industry. The remaining Mn alloy is used in the manufacturing process of handy batteries, aluminum cans, insecticides for farming, circuit boards, livestock fertilizers, coloring agents, pigments, oxidizing chemicals, sparklers, leather goods, and pharmaceuticals [26].

2.1 Ferroalloy production process

The electric arc furnace (EAF) and the blast furnace are the main approaches used to manufacture Mn alloy from all grades of Mn ore [27]. The production of ferroalloys involves multiple steps such as procuring and stockpiling raw materials, feeding them into storage

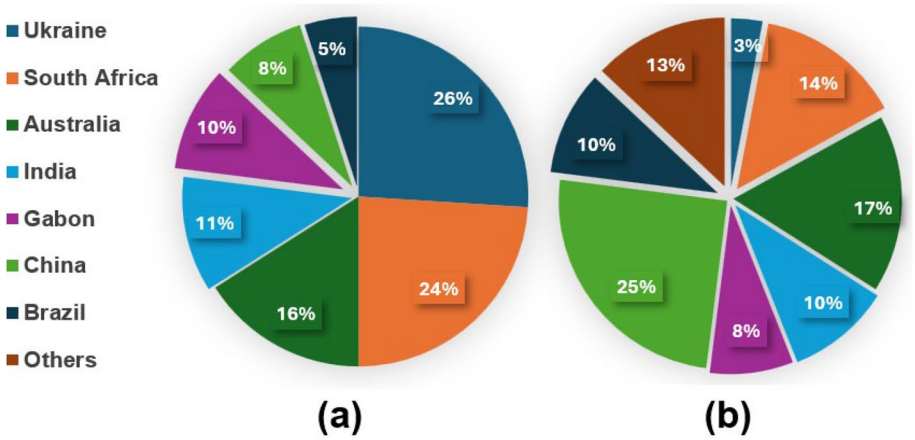

Fig. 1 World statistics. **a** Mn reserves. **b** alloy production (Adapted from: [26])

containers, transporting them to the EAF, mixing them, storing them in a furnace, smelting them, tapping the molten metal, casting it, and then cooling and handling the final product.

Figure 2 illustrates a visual representation of the movement of raw materials in a standard ferroalloy plant. To prevent the release of SiMn dust or fumes during the manufacturing process, baghouse filters are installed at smelting, tapping, ladle, casting, crushing, and screening zones [28]. However, approximately 15% of silicomanganese (SiMn) escapes as fume or dust during the entire course of converting Mn ore into alloy. Furthermore, a significant quantity of waste slag is generated during the production of the alloy. According to reports, an Indian facility produces 50 000 tons of slag from an annual alloy production of 60 000 tons. This means that approximately 900 kg of slag are generated per ton of ferroalloy manganese production, whilst 200 tons of slag are required to be disposed of every day [29]. Elsewhere, it is reported that approximately 1.2 to 1.4 tons of slag are generated for every ton of SiMn alloy produced, resulting in a yearly yield of about 10 million tons of SiMnS [30]. According to the 2012 statistics from IMnI, the globe produced approximately 15 MMT of SiMnS annually, highlighting its potential for waste valorization.

Three grades of ferromanganese alloy are used in steel manufacturing: high carbon ferromanganese (HC FeMn), refined medium carbon ferromanganese (Ref or MC FeMn), and low carbon ferromanganese (LC FeMn) or SiMn alloy. These grades have different Mn content, with HC FeMn constituting 65%–79%, Ref or MC FeMn constituting 80%–81%, and SiMn constituting 60%–77%. Out of all the grades, SiMn synthesis accounts for 56% of the entire Mn alloy production. SiMn production uses low-grade ore to manufacture 50% of global construction reinforcing steel. The global production of Mn alloys in 2000 and 2008 for HC FeMn, MC FeMn, and LC SiMn was estimated to be 3.35 and 4.73 MMT, 0.74 and 1.12 MMT, and 3.77 and 7.85 MMT, respectively, as indicated in the data in Fig. 3 [26]. The global rise in Mn alloy production over time can be attributed to the continuously growing demand for steel.

2.2 Mn concentration in ferroalloy plants

Ferroalloy industries release Mn particles into the atmosphere as aerosols during various production activities. Additionally, they produce two by-products, SiMnS and SiMnF, which are collected separately and stored in designated areas of the plant for periodic landfilling. Therefore, the World Health Organization (WHO) has limited a yearly permissible limit of 150 ng/m^3 for Mn to control

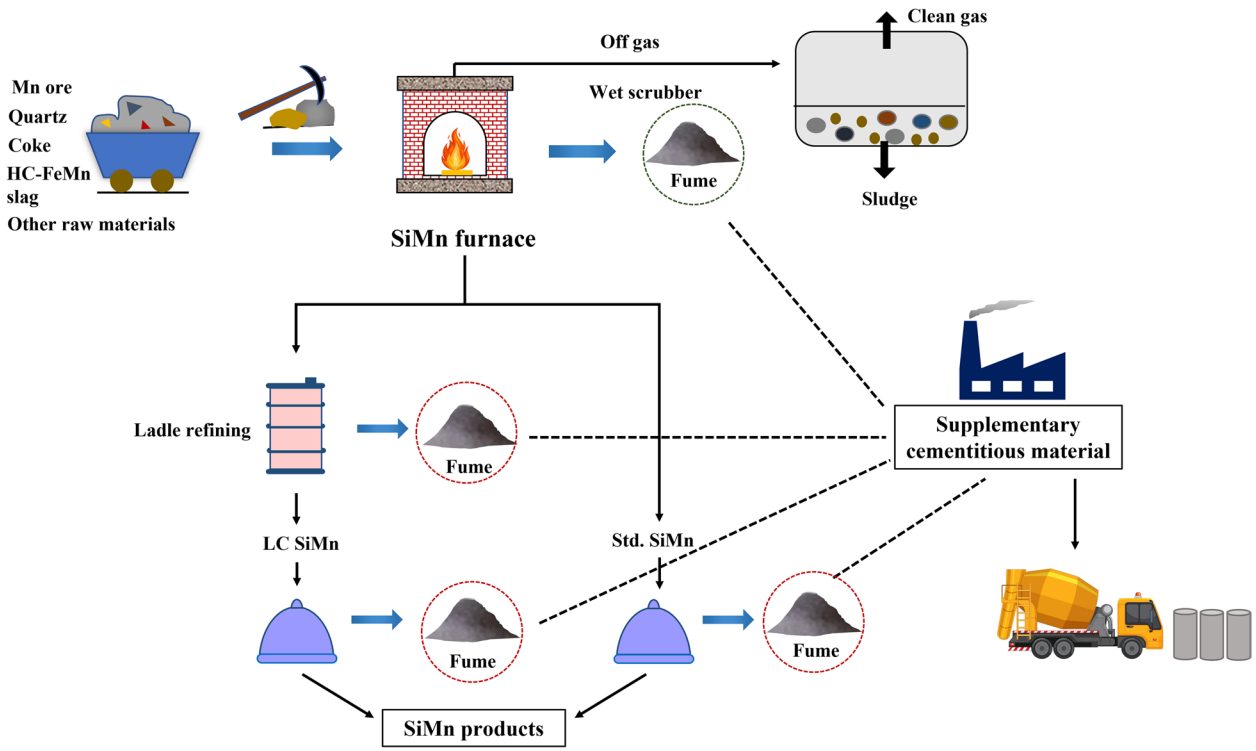

Fig. 2 Schematic of movement of unprocessed materials in a standard ferroalloy facility (Adapted and modified from: [31])

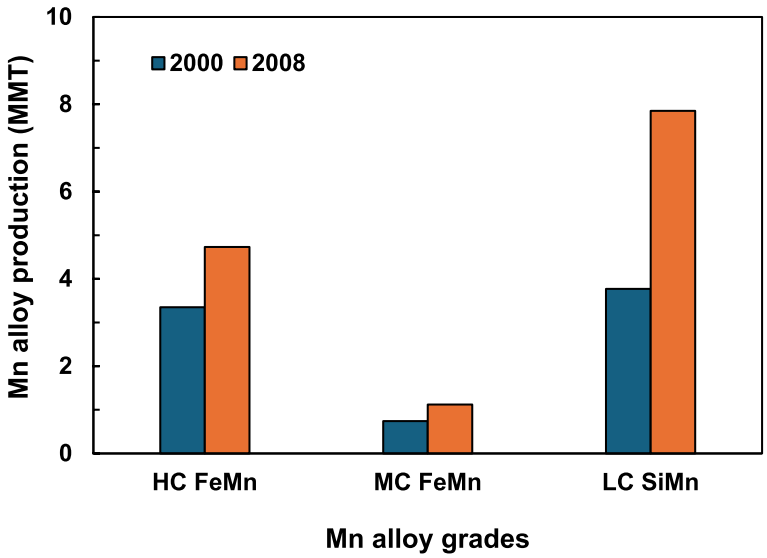

Fig. 3 Global Mn alloy production depending on grades (Adapted from: [26])

anthropogenic activities in ferromanganese refineries, which are responsible for high Mn concentration in the surrounding air of the plants. Surprisingly, this regulation is being broadly violated by many ferroalloy plants and ferromanganese refineries, as tabulated in Table 1.

2.3 Health problems associated with Mn exposure

Clinical research indicates that the human body requires only minimal amounts of Mn-based nutrients for skeletal growth, metabolic function, and regulation of the immune and nervous systems [32]. These nutrients also stabilizes hormone systems and restricts cellular oxidative stress [33, 34]. On the contrary, excessive inhalation of airborne Mn can result in various adverse health effects. It primarily affects the neurological system, leading to motor and cognitive impairments [35, 36]. Chronic exposure to Mn can lead to Mn poisoning, which bears some resemblance to Parkinson's disease [37–39]. Additionally, elevated Mn exposure in children and elderly people is particularly linked to lower intellegience quotient (IQ) levels, reduced body mass, hyperactivity disorder, and sensory deficits [40]. The Agency for Toxic Substances and Disease Registry (ATSDR) toxicological profile for Mn reports that high-level exposure has effects on the nervous system [41].

Table 1 Statistics of Mn concentration in the vicinity of some ferroalloy plants

Author(s)	Ferroalloy plant location	Average annual Mn concentration in air (ng/m^3)	Affected plant vicinity (km)	Inhabitants	Year
Haynes et al. [42]	Marietta town, USA	203	7.3 (north, north-east)	14 515	-
Ledoux et al. [43]	Agglomeration Community of Boulogne, France	7 560	-	120 000	-
Querol et al. [44]	Cantabria, northern Spain	4–23	-	-	-
Moreno et al. [45]	Santander, northern Spain	166	7 (north-east)	174 000	2007
CIMA [46]	Maliaño, Spain	781	-	10 000	2005
CIMA [47]		1 072			2009
Arruti et al. [48]	Santander, northern Spain (Mn reduction after corrective measures)	49.1	-	-	2008
Ruiz et al. [49]		31.5	-	-	2009
Hernández-Pellón and Fernández-Olmo [50]	Maliaño, Spain	714	-	-	2015

2.4 Challenges in SiMn-based recycling and processing

Conventional SiMn production and recycling methods face significant technical**,** environmental**,** and economic challenges. One of the primary issues is the high energy consumption of the process. The reduction of manganese oxides (MnO and Mn_2O_3) from ores and slags requires temperatures exceeding 1 500 ℃, typically achieved using EAFs. These furnaces have low thermal efficiency and consume vast amounts of fossil-derived energy, primarily from coke and coal. The energy intensity directly contributes to increased CO_2 emissions, making SiMn one of the more carbon-intensive ferroalloys to produce [26, 51].

From a technical perspective, material losses and inefficiencies are prevalent throughout the process. During smelting and tapping, significant quantities of Mn are lost to slag in oxidized form (MnO), which remains unreduced due to kinetic or thermodynamic limitations [52]. In addition, fine particulates such as SiMnF and dust generated from the furnace and handling operations lead to further Mn losses. These particles are often too fine or oxidized for direct reintroduction into the furnace without further processing [53]**.**

Another limitation lies in the variability and quality of input materials, especially when recycling dust, slag, or off-spec alloys. Recycled materials may contain high levels of impurities like phosphorus, sulfur, and alkalis, which compromise the quality of the final alloy and lead to greater slag volumes or environmental hazards [54]. Furthermore, the fines produced (such as SiMnF or baghouse dust) often have poor flowability and reactivity, which hinders their direct reuse without pretreatment [55].

Environmental concerns also arise from large volumes of slag and dust generated in SiMn processing. Slag management is a persistent challenge due to the limited recycling potential of high-manganese slags and their tendency to leach trace metals. Disposal via landfilling presents a long-term environmental liability, while efforts to use slag in construction or as a secondary resource are still limited in practice [56].

Economically, the low market value of recycled SiMn materials compared to primary alloys discourages investment in advanced recycling routes. While techniques such as slag reduction with ferrosilicon (FeSi) or aluminum can recover Mn, they are often cost-prohibitive due to the high prices of reductants and the energy required. Similarly, hydrometallurgical processes for recovering Mn from dust or slag are rarely implemented at scale because of their complexity, chemical cost, and waste stream management issues [57].

Finally, the lack of circular infrastructure for collecting, sorting, and processing SiMn-rich waste limits the effectiveness of recycling initiatives. Unlike steel or aluminum industries, which have established systems for scrap recovery, the SiMn industry remains relatively linear in its material flow. This makes it difficult to achieve meaningful material circularity without systemic changes, such as integrating SiMn waste streams into cement production, steelmaking, or the development of secondary alloys [56].

2.5 Leaching behavior of SiMn-based cementitious materials

The concerns regarding the leaching of heavy metals, particularly Mn, in SiMnS and SiMnF-based cementitious systems should be addressed to ensure environmental safety and compliance with regulatory standards. In response, a few recent studies have begun to explore this critical issue. Rashid et al. [58] investigated the performance of concrete incorporating up to 30% SiMnF as a cement replacement. Their findings demonstrated that Mn leaching peaked at just 0.002 mg/L within the first two days and fell below detectable limits, remaining well within safety thresholds. However, calcium leaching was significant across all mixes, with the control mix exhibiting the highest levels. Despite limited literature on SiMnF, these findings suggest its potential as a safe supplementary material when used within optimized limits.

In contrast, recent research has examined SiMnS to a greater extent. Yu et al. [59] explored the stabilization and leaching mechanisms of heavy metals in cementitious materials containing SiMnS. Their leaching assessments, conducted under simulated natural conditions, revealed that Mn was primarily present as acid-extractable species. The findings demonstrated the potential of SiMnS to safely incorporate industrial by-products while minimizing environmental risk. Zhang et al. [55] further validated the application of SiMnS in low-carbon cement formulations, where SiMnS was used alongside GBFS, flue gas desulfurization gypsum, and carbide slag. Leaching toxicity tests confirmed Mn concentrations below 0.1 mg/L in mortars with up to 80% SiMnS, and the presence of jouravskite among the hydration products indicated effective Mn stabilization under normal conditions. In contrast, Liu et al. [60] reported that although SiMnS exhibits higher hydration activity than local GBFS, it poses leaching risks under aggressive environments. While Mn concentrations in powder leachate remained within limits under neutral and mild conditions, acid leaching tests on mortars with 30%–50% SiMnS replacement revealed Mn levels as high as 31 mg/L, which suggested that environmental conditions significantly influence the leaching behavior and must be considered in durability design.

In general, current evidence suggests that SiMnS and SiMnF can be safely used in cementitious systems, with

negligible Mn leaching under normal service conditions. However, high SiMnS content and aggressive environments can elevate leaching risks, which highlighted the need for careful mix design, service condition assessment, and long-term durability evaluation to ensure safe and sustainable use. Furthermore, there remains a critical research gap regarding the leaching behavior of SiMnF-based mixes, particularly under varied exposure conditions, which should be addressed in future investigations.

3 Properties of SiMnF raw material

SiMnF varies in appearance, typically brown to brownish-black, depending on its source and processing route [61–64]. Its median particle size (D_{50}) is approximately 29.17 μm [65], comparable to that of Portland cement [66], making it viable for direct substitution. Notably, the particle size distribution often shows dual peaks at ~ 0.7 and ~ 90 μm with limited volume in between [62]; to mitigate this issue, GBFS is often blended. SiMnF has a specific gravity between 2.11 and 2.87 and a surface area ranging from 8.1 to 13.7 m^2/g. Its average moisture content is around 0.33%. While the spherical morphology improves mix flowability, its relatively low strength activity index (~ 75%) may reduce the compressive strength of cementitious composites [67]. SiMnS, in contrast, typically appears beige to dark brown, though variations from light green to nearly black have been noted due to different cooling and storage conditions [68, 69]. It has a higher specific gravity (2.90–3.02) than SiMnF, and D_{50} values ranging from 9.2 to 29.2 μm. Optimal fineness is reported in the range of 4 500–6 500 cm^2/g [70]. Table 2 depicts the common physical properties of SiMnF and SiMnS collected from previous studies.

Table 3 presents the chemical compositions of SiMnF and SiMnS reported by several previous studies. SiMnF primarily contains MnO, SiO_2, and K_2O, which collectively constitute over 70% of its mass [61, 64]. One study reported 35.42% MnO, 19.5% SiO_2, and 16.62% K_2O [61], with minor contributions from CaO (7.24%) and Al_2O_3 (1.46%). The low CaO and Al_2O_3 contents partially explain its limited strength contribution compared to more reactive SCMs like GBFS or Class C FA. Some compositions feature higher K_2O and lower SiO_2, which may influence its acid–base behavior [63, 64].

In contrast, SiMnS displays a more pozzolanic oxide composition, predominantly consisting of SiO_2, CaO, and Al_2O_3, often making up over 70% of the total mass [68, 74]. This composition supports pozzolanic reactivity, which contributes to improved strength and durability. The hydraulicity index (HI), defined as $HI = (w(CaO) + w(Al_2O_3) + w(MgO))/w(SiO_2)$, has been reported to range from 1.12 to 1.26, suggesting moderate pozzolanic activity [68, 75]. Despite this, the $w(CaO)/w(SiO_2)$ ratio (0.59–0.77) classifies SiMnS as mildly acidic [70, 76, 77]. Figure 4 depicts the SEM, EDS, and XRD of the raw SiMnF. SEM analysis reveals that SiMnF particles are generally well-rounded and vary significantly in size, with D_{10} ~ 1 μm, D_{50} between 31–94 μm, and D_{90} reaching 281 μm [78]. This wide size range may enhance particle packing and workability [79]. High-magnification SEM images [64, 80] support these observations. XRD analysis confirms the presence of manganese ferric oxide, quartz, and potassium chloride as dominant crystalline phases [64, 80].

4 Construction applications of SiMn waste

To address the negative effects of Mn found in ferroalloy industrial waste, some cement and concrete technologists have incorporated FeMn slag into the development of construction materials. Various metallurgical slags from different industrial processes, such as ferrous slag (steel slag, ferronickel slag, titaniferous slag, and stainless steel slag) and non-ferrous slag (lead slag, copper slag, nickel and nickel-copper slag, zinc slag, phosphorus slag, manganese and silico-manganese slag), have also been used as binders in construction applications [82, 83]. The following sub-sections discuss individual SiMn wastes separately.

Table 2 Physical properties of SiMnF and SiMnS

Material	Appearance	Specific gravity	Moisture content (%)	Surface area (m^2/g)	D_{10} (μm)	D_{50} (μm)	D_{90} (μm)	Average particle size (mm)	Pore volume (cm^3/g)	Shape	Ref.
SiMnF	Brown	2.87	-	10.06	0.58	29.17	179.95	-	0.0001	Spherical	[61, 62]
	Brown	2.80	-	10.00	-	30.00	-	-	-	Spherical	[63]
	Brownish black	2.11	0.32	13.70	-	-	-	0.463	-	Spherical	[64]
SiMnS	-	2.90	-	-	0.99	14.80	49.62	-	-	-	[71, 72]
	Beige to brown	2.95	-	-	-	-	-	-	-	-	[68]
	-	3.02	-	-	-	29.20	-	-	-	-	[73]
	-	2.92	-	-	-	9.20	-	-	-	-	[70]

Table 3 Chemical compositions of SiMnF and SiMnS

Material	*w*(CaO)	*w*(MnO)	*w*(SiO_2)	*w*(K_2O)	*w*(Al_2O_3)	*w*(SO_3)	*w*(MgO)	*w*(Fe_2O_3)	*w*(Na_2O)	*w*(Cl)	*w*(ZnO)	*w*(TiO_2)	LOI	Ref.
SiMnF	7.24	35.42	19.50	16.62	1.46	6.24	5.71	3.35	-	-	-	-	5.82	[61]
	4.93	34.10	15.78	27.25	1.76	6.32	5.10	2.37	1.73	-	-	-	5.40	[64]
	7.00	31.00	22.00	17.00	2.00	8.00	9.00	2.00	-	-	-	-	-	[78]
SiMnS	29.10	12.23	36.53	1.08	9.86	2.77	4.69	0.92	0.34	-	-	-	1.25	[70]
	26.17	10.06	40.33	-	14.55	-	5.74	0.75	-	-	-	-	2.36	[71, 72]
	25.20	9.90	42.60	2.20	12.20	0.12	4.20	1.00	0.36	-	-	0.36	-	[69, 74, 76, 81]
	20.00	20.40	32.30	-	16.10	-	4.55	0.30	-	-	-	-	-	[68]
	29.30	10.29	38.17	0.76	14.78	0.12	2.77	1.79	0.42	-	-	-	1.12	[77]
	17.74	11.23	36.40	-	25.94	-	4.27	1.20	-	-	-	0.12	2.20	[73]
	25.42	11.90	37.67	-	11.73	1.70	4.02	1.22	0.21	-	-	0.24	-	[75]

LOI denotes loss on ignition

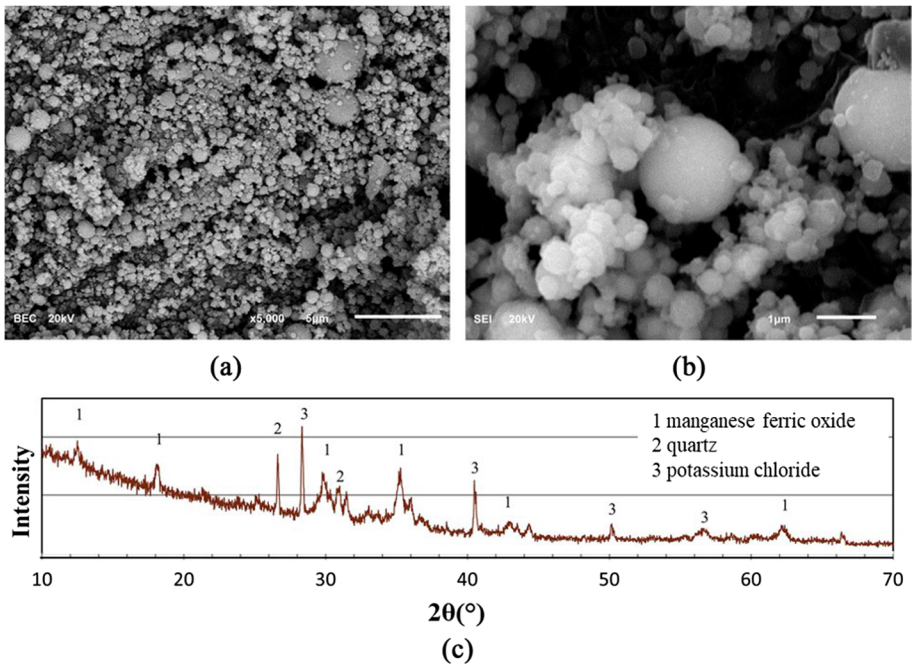

Fig. 4 Characterization of the raw SiMnF. **a** Wide range, well-rounded particles [78]. **b** High magnification view [64, 80]. **c** XRD spectrum [64, 80]

4.1 SiMnS-based binders

To the best of recent knowledge, only a few studies have been conducted hitherto on SiMnS-based waste material as cementitious composites or binders [56, 69, 71–74, 76, 77, 81, 84–87]. It was observed that all these studies on SiMnS were conducted after its pre-treatment in the laboratory since the slag is produced in coarse form, which at least requires extensive pulverization. These studies mainly focused on the reaction kinetics, pozzolanic activity, and structural reorganization of SiMnS, while others evaluated aspects such as shrinkage, durability, and electrochemical characteristics. Studies from 1999 to 2016 partially replaced traditional PC with SiMnS, which cannot effectively mitigate the negative effect of PC production, while the remaining studies in subsequent years attempted to develop alkali-activated binder (AAB) [88]; however, the AAB mainly consisted of GBFS or FA as a primary SCM and a minor amount of ferroalloy by-product.

Research on SiMnS waste in infrastructural applications demonstrated that it can be activated through mechanical, thermal, and/or chemical processes to enhance its reactivity. Studies indicate the possibility of partially replacing PC with up to 50% SiMnS [29, 69, 71, 76, 77, 81, 85, 86]. The positive effects of SiMnS, after pre-treatment by milling [74, 77], air or water cooling of slag, and various curing methods on the reaction mechanism and rate of strength development of the produced binder, were investigated [29, 87, 89]. Some research explored the potential of formulating AAB using 100% SiMnS [74, 89], SiMnS admixed with FA [72, 73], and SiMnS admixed with high volume GBFS [84]. It was revealed that the presence of reactive lime content could enable the dual formation of calcium aluminosilicate hydrate (C-A-S–H) and N/C-A-S–H phases in the binder matrix, resulting in improved mechanical strength of SiMnS-based AAB [73]. Additionally, resistance to reinforcement corrosion was evident when SiMnS blended with GBFS was used as precursor to the AAB [84]. X-ray analysis also showed the formation of hydrated calcium manganese (C-Mn-H) compounds responsible for enhancing the mechanical properties of the cementitious product [76].

4.2 SiMnF-based binders

Very few studies have been reported so far on SiMnF as a cementitious or precursor material, as this waste material is relatively novel and was recently identified. Most research has focused on the synthesis and evaluation of alkali-activated SiMnF-based paste and mortar [67, 80, 90, 91]. These studies generally found that SiMnF possesses poor reactivity ascribed to the abundance of Mn, Si, and K based oxides and a deficiency of CaO, in contrast to the SiMnS. The subsequent sections provide the first comprehensive review of SiMnF-based cementitious composites.

The first phase of the review examines the physicochemical and microstructural characteristics of SiMnF,

emphasizing its distinctions from SiMnS. The second phase explores the synthesis of SiMnF-based PC and alkali-activated binders, along with their synergies with other SCMs. Subsequently, the influence of key fresh and hardened properties, including durability of the developed binders is investigated. Next, the mineralogy, morphology, bond behavior, and thermal stability of the developed binders, as identified by advanced analytical tools, are reported. In the fourth phase, a sustainability analysis was carried out on all the SiMnF-based mixtures in the literature, employing life cycle assessment (LCA). Finally, the challenges and gaps in literature are highlighted, and a roadmap to promote and upscale the SiMnF-based binder technology is presented. This review is intended to serve as a guide for the engineers to establish safe valorization strategies for this newly identified SiMnF from ferroalloy plants for infrastructural applications. This comes at a time when established SCMs, such as FA, are experiencing declining production capacity compared to demand, necessitating the investigation of other potential SCMs. It is also envisioned that this review will provide opportunities for extending future research in this domain, leading to further improvements in the engineering properties. Most importantly, this review will contribute to achieving solid waste management, net-zero targets, low-carbon construction, and a construction circular economy.

4.3 Mixture synthesis of SiMnF

According to the literature, SiMnF was used to formulate both traditional and alkali-activated concretes. However, self-compacting concrete (SCC) with a conventional design using the absolute volume method has also been reported [64]. In that research, SiMnF was introduced to the mixtures by partially replacing the cement (10%–90%). The water/binder ratio was maintained at 0.40 in all mixtures, while the superplasticizer (SP) dosage was varied to achieve a desirable flow (670–680 mm). To ensure the high cohesiveness of SCC-SiMnF mixtures, 20% of the sand was replaced by limestone powder. Water immersion for 28 days was adopted as a curing method for the developed SCC-SiMnF mixtures.

The majority of previous studies used alkali activators, namely NaOH (SH) and Na_2SiO_3 (SS), to activate SiMnF. Nasir et al. [62] conducted a study utilizing activated SiMnF with SH and SS. Different concentrations of SH (4, 8, 10, 12, and 16 M) and different SS/SH ratios were tried for optimization purposes. In another study, concentration and SS/SH ratio were maintained at 10 M and 2.5, respectively, while SiMnF content was partially replaced with GBFS [92]. Free water (FW) was added to the mix to facilitate the chemical reaction in several research articles [61–63, 92–94]. However, other researchers do not incorporate FW [80]. In addition to the conventional experimental design, the Taguchi method was used to formulate and manage the effective variables of the mix design [67, 90]. The effects of the previously mentioned parameters and mix design variables on the fresh and hardened properties of alkali-activated mortars are discussed in the subsequent sections.

5 Fresh and hardened properties

In this section, an exploration of the fresh properties of mortar/concrete mixtures containing SiMnF, including aspects such as flow and setting time, has been undertaken. The discussion extends to the mechanical properties of SiMnF composites, including compressive, tensile, and flexural strengths as well as modulus of elasticity. Through an in-depth examination of these properties, the key factors to produce high-performance SiMnF mortar/concrete have been highlighted.

5.1 Rheological properties

As detailed in Sect. 3, SiMnF exhibited spherical particles similar to FA, which is expected to enhance the flowability of the mix through a lubrication effect. However, the high fineness of SiMnF may increase the demand for water to achieve comparable flow, rendering an overall loss in flowability from the inclusion of SiMnF at a constant water/binder ratio. It was reported that there is a demand to increase the dosage of SP with an increase in the quantity of SiMnF in SCC to maintain a perfect slump flow between 670 and 680 mm [64]. To achieve that, SP doses ranging from 0.80% to 1.06% were introduced to SCC mixtures containing SiMnF, replacing 10% to 90% of the cement. Other workability tests, such as T50 flow time, V-funnel time, L-box ratio, and U-box were estimated. The control mixture exhibited the highest T50 flow time (4.5 s), while this time decreased and reached 2 s, the minimum limit by EFNARC [95], at 70% SiMnF content. Similarly, the V-funnel time of the control mixture was 11.5 s, while it was 6 s, the minimum limit by European Federation of National Associations Representing Producers and Applicators of Specialist Building Products for Concrete (EFNARC) [95], for a 70% SiMnF mixture. Mixtures containing 80% and 90% SiMnF fail to pass these two tests. However, all mixtures (10%–90% SiMnF) pass the L-box and U-box tests with similar enhancement trends of the filling ability. Paste samples were prepared to examine the initial and final setting times. The control mixture resulted in 140 and 225 min for the initial and final setting times, respectively. The incorporation of SiMnF increased both the initial and final setting times significantly. The initial setting time of mixtures containing 10%–90% SiMnF ranged from 172 to 470 min, while the final setting time ranged from 285 to

720 min. In other research [67], it was reported that the incorporation of 40% SiMnF to replace cement exhibited no negative effect on the flowability of cement composites; however, the incorporation of 10% SF resulted in a severe reduction in the flowability.

In alkali-activated mixtures, factors such as SH molarity, SS/SH ratio, and alkaline activators to precursor materials ratio (AAs/PMs) are crucial to the flowability. Najamuddin et al. [80] studied the effect of SH molarity (4 M, 8 M, 12 M) and SS/SH (2.0, 2.5, 3.0) ratios on the flow of alkali-activated mixtures. Generally, it was found that flow increased with an increase in SH molarity; however, it is also controlled by the SS/SH ratio. The optimum silica modulus (SiO_2/Na_2O) is the key factor in achieving the highest flow. For example, using 8 M of SH and SS/SH = 2.0 yields the highest flow due to the optimum ratio of SiO_2/Na_2O (1.53). The mix with 12 M of SH and a 2.0 SS/SH ratio results in a lower flow due to a disproportionate SiO_2/OH ratio. Another study examined the effect of the AAs/PMs ratio (0.50, 0.51, 0.52, and 0.53) on the flow of SiMnF mortars [90]. The findings revealed that the flow is always better with higher AAs/PMs ratios.

Nasir et al. [92] fixed the molarity of SH at 10 and the silica modulus at 3.3 and varied the quantity of SiMnF by replacing it with GBFS at 10%, 20%, 30%, 40%, and 50%. A gradual decreasing trend in the flow was observed as the replacement level increased. For example, the flow diameter was reduced from 170 to 139 mm when 40% of SiMnF was replaced by GBFS. This reduction was attributed to the fact that the angularity of GBFS particles is considerably higher compared to the spherical shape of SiMnF particles, which creates friction resistance during flow. Another observation of replacing SiMnF with GBFS was the significant drop in the initial and final setting times. The control mix recorded 470 and 525 min for the initial and final setting times, respectively. However, replacing 50% of the SiMnF with GBFS decreased the initial and final setting times to 20 and 30 min, respectively. This huge reduction in the setting times was attributed to the rapid formation of C-A-S–H and the formation of calcium carbonate ($CaCO_3$) due to the excessive quantity of calcium oxide (CaO) available in the GBFS and its reaction with calcium dioxide (CO_2) in the surrounding atmosphere.

5.2 Mechanical properties

5.2.1 Cement-based SiMnF concrete

The hardened properties of cement-based SiMnF SCC were investigated by Gawah et al. [64]. Figure 5 depicts the mechanical properties, including compressive strength, split tensile strength, flexural strength, and modulus of elasticity of cement-based SCC containing 10%–70% SiMnF. All mechanical properties followed a similar trend, increasing up to 20% SiMnF, then gradually decreasing as SiMnF content increased. According to Gawah et al. [64], the strength and stiffness of the 10% and 20% SiMnF mixtures improved significantly due to the packing effect, where the finer particles of SiMnF effectively occupy the voids between the larger aggregate particles as well as cement. This interpretation is further supported by the wide particle size distribution and spherical morphology of SiMnF particles, as described in Sect. 3, which enhance packing efficiency and reduce voids [78]. However, once the amount of SiMnF exceeds 20%, the strength and elastic modulus show a decreasing trend. This decline can be attributed to the potential increase in the surface area of fine SiMnF particles, leading to insufficient cement binding for these particles.

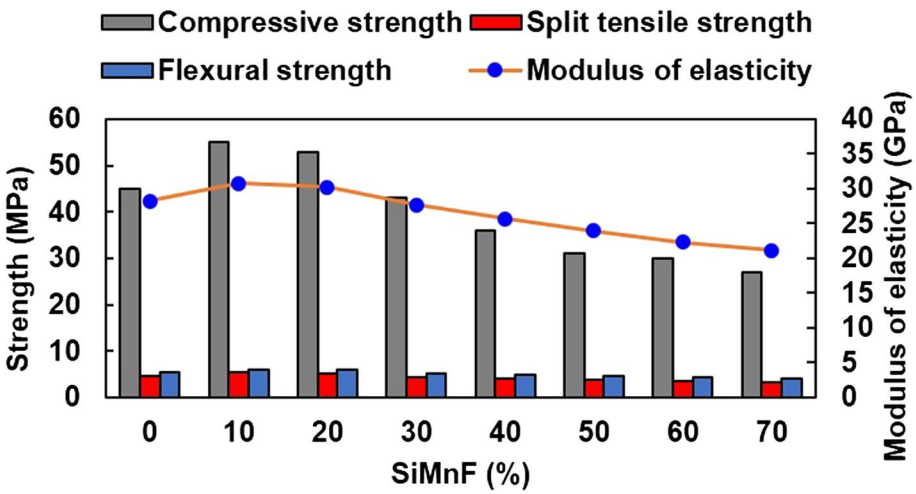

Fig. 5 Mechanical properties of cement-based SiMnF SCC (at 28 days of curing) [64]

Consequently, the 10% SiMnF mixture exhibited an increase in compressive strength, split tensile strength, flexural strength, and modulus of elasticity by 22%, 14%, 17%, and 9%, respectively. Furthermore, the 70% SiMnF mixture exhibited a decrease in compressive strength, split tensile strength, flexural strength, and modulus of elasticity by 39%, 31%, 26%, and 25%, respectively. This reduction in the compressive strength is attributed to the low reactivity of SiMnF compared to other pozzolanic materials. In the same line, the effect of incorporating SF along with SiMnF was investigated [67]. It was found that the addition of SF can compromise the reduction in the compressive strength of mixtures with only SiMnF.

5.2.2 Alkali-activated-SiMnF-based mortar

Few previous studies investigated the performance of alkali-activated SiMnF-based mortars. This section presents and discusses in detail the mechanical properties of alkali-activated-SiMnF-based mortars. A recent study by Ibrahim et al. [96] investigated the incorporation of SiMnF into alkali-activated binder systems, replacing part of the ground volcanic pumice. The inclusion of 30% SiMnF resulted in a compressive strength of 48.15 MPa after 28 days of ambient curing, alongside notable improvements in the microstructure. These findings further support the potential of SiMnF to contribute positively to the strength development of binder systems under suitable activation conditions. As compressive strength is considered the main mechanical property of concrete, researchers optimized the mix design parameters based on compressive strength results. The compressive strength of alkali-activated-SiMnF-based mortars was investigated using different concentrations of SH (4, 8, 10, 12, and 16 M) and SS/SH ratios (1, 1.5, 2, 2.5, 3, and 3.5) [62]. In the first set of experiments, the SS/SH ratio was fixed at 2.5, while the molarity of SH ranged from 4 to 16 M. In the second set of experiments, the molarity of SH was fixed at 10, while the SS/SH ratio ranged from 1 to 3.5 M. Figure 6 depicts the compressive strength of SiMnF alkali-activated mortar for different SH molarities and SS/SH ratios [62]. The lowest compressive strength (33.1 MPa) was recorded at the lowest concentration of SH (4 M). The compressive strength increases as the concentration of SH increases up to 10 M (44.5 MPa); however, strength declines with a further increase in the concentration of SH. This indicates that 10 M is the optimum concentration of SH to produce alkali-activated SiMnF concrete. At this concentration, hydroxylation and dissolution are at their optimum levels, resulting in better polymerization. Regarding the effect of the SS/SH ratio, the compressive strength increases with the increase of the SS/SH ratio up to 2.5, showing the highest strength (44.5 MPa); however, a degradation in the compressive strength was observed as the SS/SH ratio increased, reaching the lowest strength (29.6 MPa) at 3.5. This degradation is attributed to the precipitation of excessive silicate that disturbs polymerization and prevents the dissolution of SH. For three different molarities (4, 8, and 12 M), Najamuddin et al. [80] reported that the flexural strength of alkali-activated-SiMnF-based mortars was the highest (3.18 MPa) using 8 M of SH. This observation is a good match with the trend of compressive strength results.

The effect of the AAs/PMs ratio on the compressive strength of alkali-activated-SiMnF-based mortars was investigated using different ratios (0.5, 0.51, 0.52, and

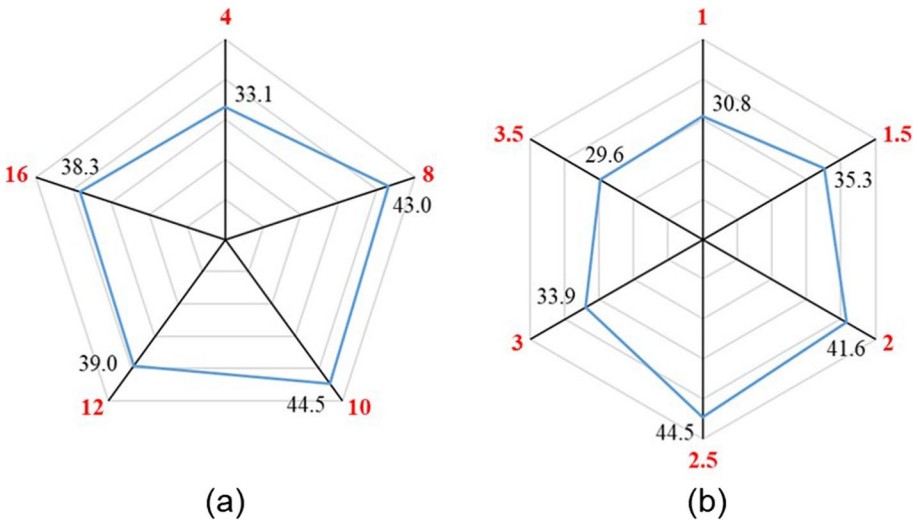

Fig. 6 Effect of activator parameters on the compressive strength (in MPa) of SiMnF alkali-activated mortar. **a** SH molarity. **b** SS/SH ratio [62]

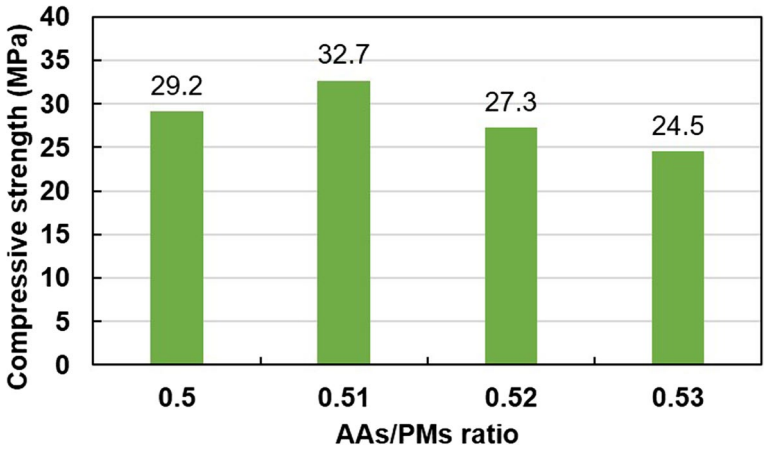

Fig. 7 Effect of AAs/PMs ratio on the compressive strength of SiMnF alkali-activated mortar [90]

0.53) [90]. Figure 7 depicts the compressive strength of SiMnF alkali-activated mortar for different AAs/PMs ratios. The highest compressive strength was 32.7 MPa, achieved using a 0.51 AAs/PMs ratio. This combination of a mixing ratio can be considered optimal. The mixture with the highest AAs/PMs ratio (0.53) showed a low compressive strength (24.5 MPa) due to the high sand/PMs ratio, while the mixture with the lowest AAs/PMs ratio (0.5) showed a relatively low compressive strength (29.2 MPa) due to the insufficient dissolution of SiMnF. Overall, decreasing the alkaline activator content results in a marginal reduction in the compressive strength; however, increasing the alkaline activator content causes a considerable reduction in the compressive strength. This reduction is attributed to the excessive dissolution rate of SiMnF, which slows down the polycondensation rate later on [97].

The curing regime is another factor that affects the compressive strength of alkali-activated-SiMnF-based mortars. The effect of heat curing on the compressive strength of alkali-activated-SiMnF-based mortars using different temperatures (40, 60, 80, and 95 ℃) and different periods (3, 6, 12, and 24 h) was studied [93]. To optimize these variables, two sets of experiments were executed. In the first set, the temperature varied, while the period was fixed at 6 h. In the other set, the period was varied, while the temperature was fixed at 60 ℃. The 3-day compressive strength values of the control mixtures cured in water and at room temperature were 23.4 MPa and 23 MPa, respectively. Figure 8 depicts the 3-day compressive strength of alkali-activated-SiMnF-based mortar for different curing temperatures and periods. The early strength tends to increase with rising curing temperatures up to 60 ℃, reaching a strength of 37.8 MPa. Beyond this point, however, the compressive strength exhibits a decreasing trend with further increases in curing temperature. On the other hand, a significant increase in compressive strength was observed when the curing period was extended from 3 to 6 h. Further increase in the curing period to 12 and 24 h improved the compressive strength marginally. Therefore, the optimal curing parameters are identified as 60 ℃ and 6 h, which allows for the attainment of 83.5% of the 28-day strength within 3 days only.

6 Microstructural analysis

The microstructure of SiMnF-based cementitious composites is a critical determinant of their mechanical strength, durability, and long-term performance in construction applications. Since SiMnF is an industrial byproduct with variable chemical composition and particle morphology, understanding its interaction within cementitious matrices is essential for optimizing material design. The microstructural evolution of these composites is governed by multiple factors, including the alkali activation process, the incorporation of SCMs, curing conditions, and the inherent reactivity of SiMnF particles. A comprehensive analysis of pore structure, crack propagation, interfacial transition zones (ITZs), and reaction products provides valuable insights for engineering high-performance, sustainable construction materials.

6.1 SEM analysis

SEM is a powerful tool for characterizing the microstructural features of SiMnF-modified cementitious composites at high magnification. SEM imaging reveals critical details about particle morphology, distribution, bonding mechanisms, and porosity, each of which influences mechanical behavior and durability. By examining these microstructural attributes, researchers can establish

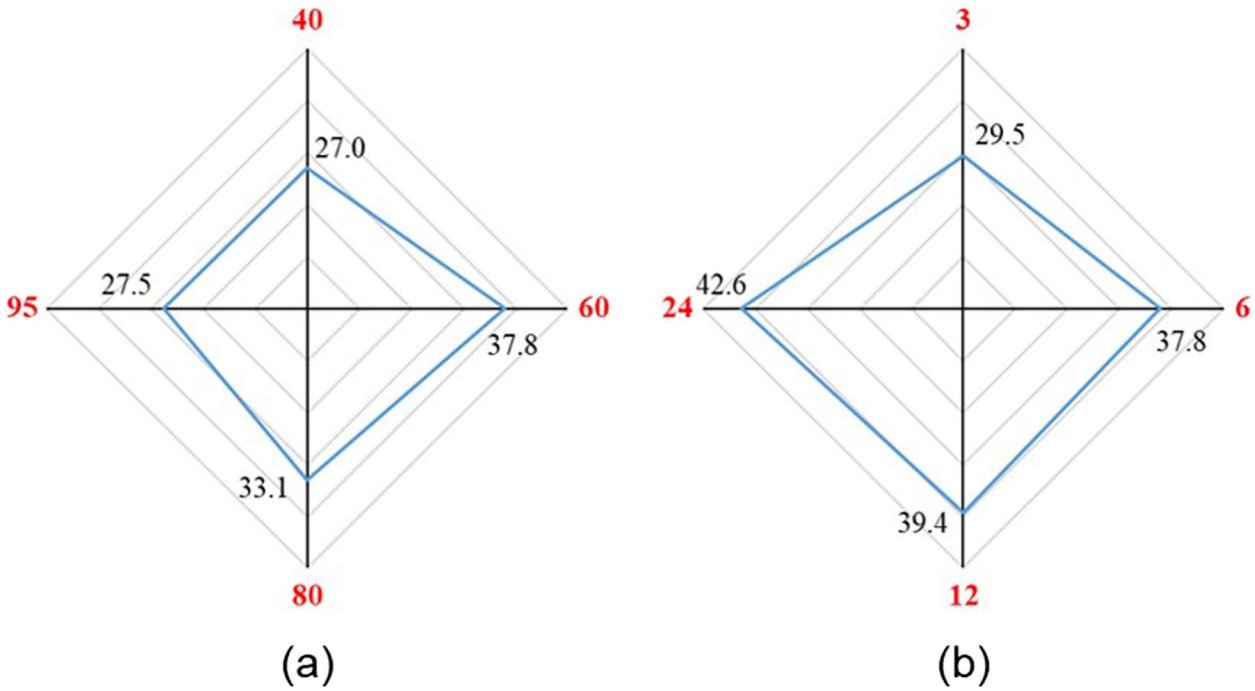

Fig. 8 Effect of heat curing parameters on the compressive strength (in MPa) of SiMnF alkali-activated mortar. **a** Curing temperature (°C). **b** Curing period (hours) [93]

correlations between processing parameters and material performance, enabling the development of tailored composites for specific applications.

The alkali activation of SiMnF is highly dependent on the concentration of the alkaline solution and the silica modulus (SiO_2/Na_2O ratio). Najamuddin et al. [80] investigated the effect of NaOH molarity on SiMnF-based geopolymers and found that a lower molarity (4 M) at an optimum silica modulus ratio of 2.5 resulted in a loosely packed microstructure with visible porosity and minimal cracking (Fig. 9(a)). This can be attributed to insufficient hydroxyl ions (OH^-) to fully dissolve silica and alumina species from SiMnF, leading to partial geopolymerization and unreacted residues. Conversely, a higher NaOH concentration (12 M) facilitated greater silica dissolution, promoting the formation of a dense sodium aluminosilicate (N-A-S–H) gel matrix. The increased gel formation filled interstitial voids, reducing porosity and enhancing mechanical strength. However, excessive alkalinity also induced microcracking due to rapid geopolymerization and shrinkage stresses. This suggests that an intermediate molarity (~8–10 M) may offer the best compromise between densification and crack mitigation.

Since SiMnF is primarily a silica-rich material with limited calcium content, its reactivity in cementitious systems can be enhanced by blending it with calcium-rich SCMs such as GBFS. It was demonstrated that pure SiMnF geopolymers exhibited weak bonding, wide cracks, and residual unreacted particles due to insufficient calcium for cross-linking in the geopolymer network [92]. However, replacing 30% of SiMnF with GBFS, which supplies additional CaO, led to the formation of calcium aluminosilicate hydrate (C-A-S–H) gel alongside N-A-S–H gel, improving microstructure cohesion (Fig. 9(b)).

Heat curing further optimized the reaction kinetics, as seen in Fig. 9(c) [63], where specimens cured at 60 ℃ exhibited a more refined microstructure with narrower, discontinuous cracks. This improvement is attributed to accelerated polycondensation and better gel interconnectivity under thermal activation.

The durability of SiMnF-GBFS composites under sulfate exposure was examined by Nasir et al. [61]. They observed that low-molarity (4 M) specimens suffered severe microstructural degradation when exposed to $MgSO_4$ solution, with visible cracking and gel depolymerization. In contrast, high-molarity (10 M) GBFS-modified specimens maintained structural integrity due to their compact microstructure, which impeded sulfate ion penetration. This highlights the importance of optimizing alkali concentration and SCM selection for enhanced durability in aggressive environments.

To further enhance microstructure densification, Nasir et al. [67] incorporated SF into SiMnF-based composites.

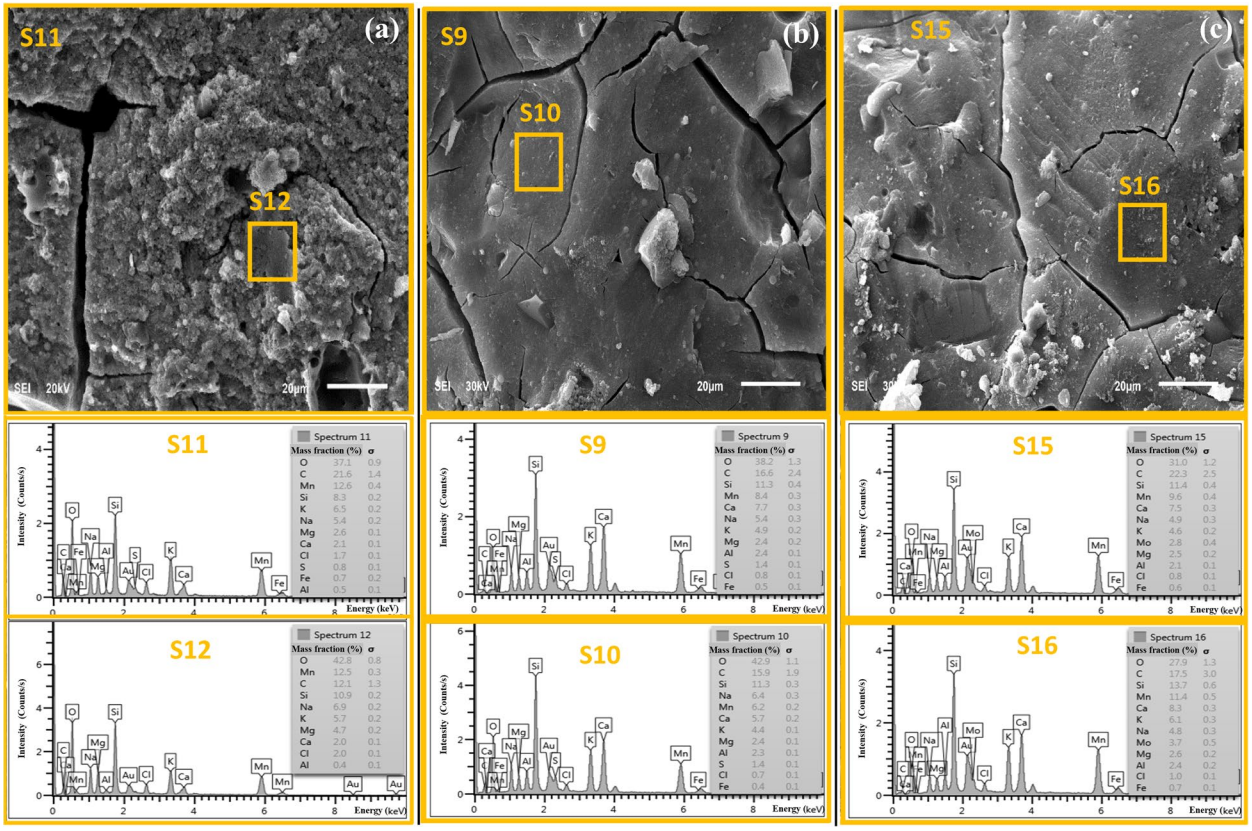

Fig. 9 SEM micrographs of alkali-activated binders. **a** Low-temperature cured SiMnF (100%). **b** Low-temperature cured 30% GBFS blended. **c** Heat cured at 60 °C [63]

While SiMnF alone introduced some porosity due to its irregular particle packing, the addition of 5% SF, a highly reactive pozzolan with ultrafine particles, effectively filled nano-scale voids and promoted secondary C-S–H gel formation. This led to a more homogeneous microstructure with reduced permeability, improving both mechanical strength and chemical resistance.

Curing conditions significantly influence the reaction kinetics and final microstructure of SiMnF composites. It was found that oven curing at 60 ℃ for 6 h maximized geopolymerization, yielding a dense and well-connected gel network [93]. However, prolonged heating (> 6 h) or higher temperatures (> 80 ℃) caused excessive water evaporation, leading to capillary pore formation and strength reduction. Ambient curing, while energy-efficient, produced a less homogeneous microstructure due to slower reaction rates, emphasizing the need for controlled thermal treatment in industrial applications.

6.2 EDS analysis

Elemental analysis is a valuable technique for characterizing SiMnF in a cementitious matrix. This information is essential for understanding the composition of SiMnF. By determining the elemental composition of SiMnF, crucial insights into its chemical makeup can be gained, which directly influence the behavior and properties of the cementitious matrix. It also helps to establish relationships between specific elements and material properties by correlating the elemental composition of SiMnF with the performance of the cementitious matrix. This knowledge enables targeted adjustments to the composition to achieve the desired performance characteristics. Najamuddin et al. [80] conducted EDS analysis on alkali-activated SiMnF mortar, revealing the presence of several major and moderate elements. The major elements identified included silicon (Si), sodium (Na), manganese (Mn), and potassium (K), while chlorine (Cl), magnesium (Mg), and calcium (Ca) were present in moderate quantities. Additionally, sulfur (S) and aluminum (Al) were traced at lower levels. The strength development of the mortar was found to be influenced by the ratios of Si/Mn and Na/Mn, with favorable strength observed at ratios higher than 0.6 and 0.35, respectively. This favorable development was attributed to the chemical changes in reaction products with alkali activators at these concentrations.

Furthermore, the degree of polymerization and transformation of reaction products was observed to be more pronounced at higher concentrations of alkali activators

compared to mild concentrations, as shown in the ternary diagram in Fig. 10(a). An analysis of the elemental composition of alkali-activated SiMnF binders was conducted, and crucial factors indicating binder performance were identified [92]. Specifically, the ratios of Ca/Si, Si/Mn, and Ca/Mn were found to be significant. Specimens with higher ratios of Ca/Mn, Si/Mn, and Ca/Mn (0.95, 1.30, and 1.23, respectively) exhibited a denser microstructure compared to specimens with lower ratios (0.25, 0.66, and 0.16, respectively) when cured at room temperature. This difference in microstructure indicated varying levels of strength development. Moreover, the impact of heat curing on alkali-activated SiMnF composites, particularly when replaced with 30% of GBFS, was demonstrated [63]. Heat curing facilitated enhanced reactivity of calcium (Ca) with other major elements of precursors and increased the amorphous nature of the reaction products. This resulted in higher early-age strength development. Conversely, heat curing of pure alkali-activated SiMnF led to lower strength development due to its high Mn/Ca ratio, indicating that Mn-bearing particles were less activated by heat curing.

6.3 XRD analysis

XRD analysis plays a crucial role in characterizing the crystalline structure and phase composition of SiMnF composites, providing valuable insights into their properties, reactivity, and performance. Najamuddin et al. [80] highlighted the importance of specific activation conditions for the successful formation of

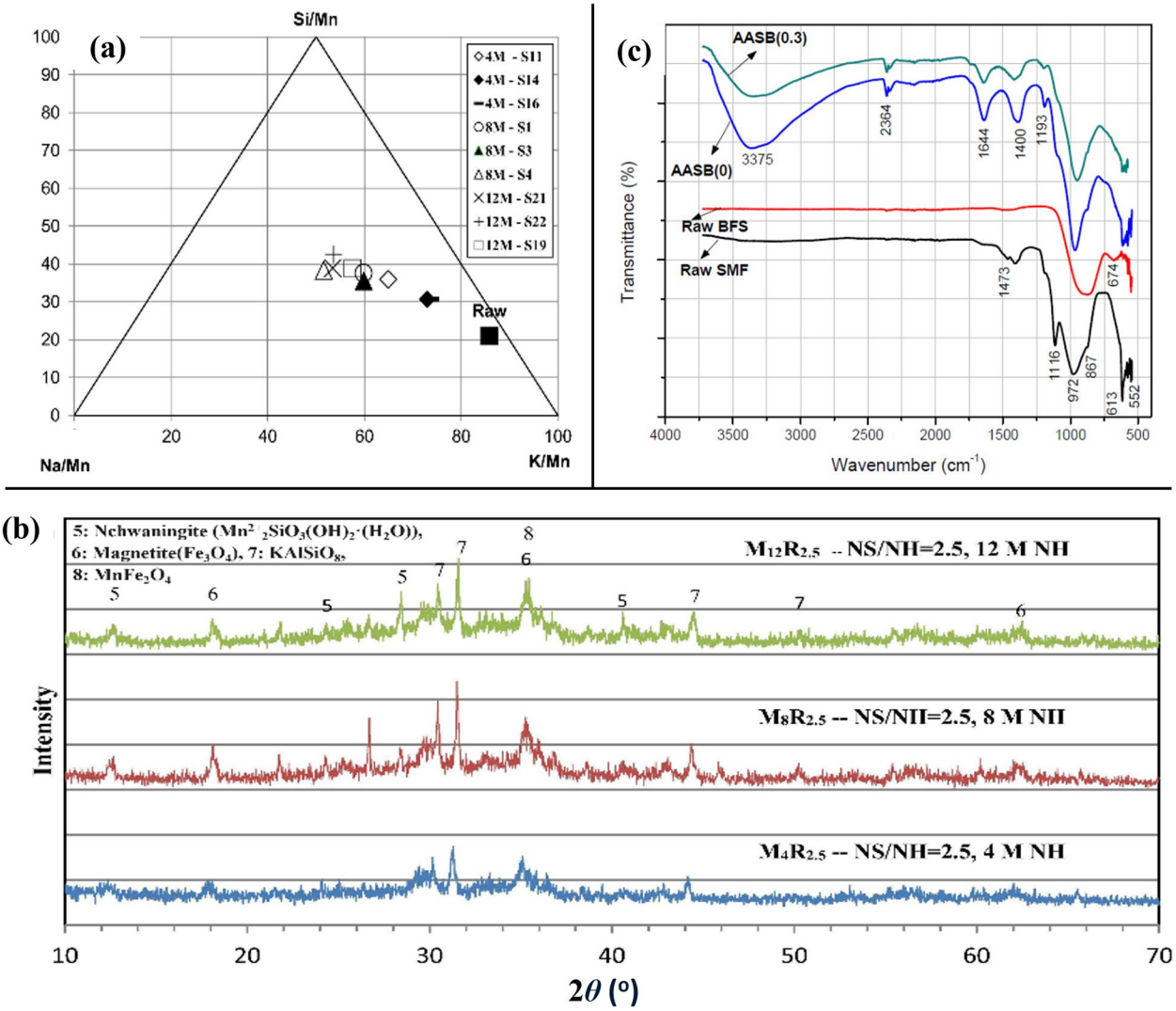

Fig. 10 Composition of raw and alkali-activated SiMnF. **a** Ternary diagram of Si, Na, and K compositions normalized to Mn. **b** XRD diffractogram of alkali-activated SiMnF specimen with varying NaOH molarity [80].**c** FTIR spectrum of alkali-activated SiMnF composite with 0% GBFS ($AASB_0$) and 30% GBFS ($AASB_{0.3}$) [92]

key geopolymerization products in SiMnF composites. They found that a higher concentration of NaOH (12 M) and an optimum ratio of Na_2SiO_3/NaOH (2.5) are crucial for activating the manganese compound in the presence of soluble silica. This activation process led to the formation of nchwaningite ($Mn_2^{2+}SiO_3(OH)_2{\cdot}(H_2O)$), a primary geopolymerization product responsible for enhancing the density, strength, and stability of the composite (as shown in Fig. 10(b)). Additionally, the geopolymerization process resulted in the formation of other important products such as magnetite (Fe_3O_4), manganese iron oxide ($MnFe_2O_4$), and $KAlSiO_8$. These findings underscore the significance of optimizing activation conditions to promote the formation of desired geopolymerization products in SiMnF composites. It was found that subjecting SiMnF to alkali activation led to the formation of glaucochroite and nchwaningite minerals [92]. Additionally, the inclusion of GBFS in the alkali-activated SiMnF binder was observed to increase the reactivity between potassium oxide and calcium oxide (CaO), as well as silicon dioxide (SiO_2). This increased reactivity resulted in the formation of potassium feldspar (K-A-S–H), which contributed to the development of a denser microstructure and consequently improved strength. Moreover, the GBFS incorporation refined the pores and densified the microstructure, which resulted in reduced carbonation, as evident from the disappearance of the calcite peak in specimens with 30% GBFS compared to those of control specimens.

Furthermore, research findings indicated that the XRD diffractogram of SiMnF composite was more crystalline than that of GBFS admixed SiMnF composite cured at room temperature, while heat curing at 60 ℃ further reduced the crystallinity of the GBFS admixed SiMnF composite [63]. The formation of calcite (21.9°), and the increased crystallinity of hydrotalcite peaks indicates carbonation in the control mix. Notably, the strength developed in these alkali-activated binders was due to the presence of nchwaningite, glaucochroite, feldspar, tobermorite, stratlingite, and C-S–H products. The enhancement in strength in 30% GBFS incorporated specimens is attributed to the formation of stratlingite, additional peaks of C-S–H (~ 50.4°), feldspar (~ 50.4°), and increased crystallinity of C-Mn-H and C-S–H phases (~ 29.6°). Further, heat treatment enhanced the amorphousity of the 30% GBFS-incorporated specimens, resulting in a reduction in the intensity of products such as tobermorite, feldspar, C-S–H, and hydrotalcite, while the stratlingite peak disappeared, which favored the high-early strength development. Nasir et al. [61] reported that upon exposure to sulfate attack, the unreacted Ca^{2+} cations and Ca-based products in the alkali-activated SiMnF binders reacted with the SO_4^{2-} anions supplied by $MgSO_4$, resulting in the formation of deterioration products, namely, thenardite, gypsum, and thaumasite. Because of the absence of gypsum/brucite phases in the control specimen due to a lack of CaO content or Ca-based products compared to that of GBFS-admixed specimens, the resistance to sulfate attachment was higher in the control than in GBFS-incorporated specimens. However, among the GBFS-incorporated specimens, the deterioration against sulfate attack was more prominent with the formation of high crystallinity of gypsum, brucite, and calcite in low-molarity (4 M) specimens than in high-molarity (10 M).

6.4 FTIR analysis

FTIR analysis showed that the incorporation of GBFS reduced the excessive carbonation (CO_3^{2-} at 1 400 cm^{-1}), weak hydroxyl compound (-OH at 3 375 cm^{-1}), and bonded water molecule (H–O-H at 1 644 cm^{-1}) in alkali-activated SiMnF composites. This reduction was attributed to the pore-filling effect of GBFS, which decreased the microcracks and enhanced the density of the microstructure (as shown in Fig. 10(c)) [92]. It was observed that when the alkali-activated specimens were subjected to $MgSO_4$ exposure, absorption peaks of gypsum bonds (S–O) at 600, 670, and 1 130 cm^{-1} with increased crystallinity were noted with an increase in the GBFS content or a decrease in the molarity among the GBFS-incorporated specimens [61]. Thus, the lower gypsum formation, decalcification, and dealumination of the control mix were due to less CaO and Al_2O_3 compared to the GBFS-admixed specimens. The strong stretching vibration (3 325 cm^{-1}) in low-molarity GBFS specimens compared to those of high-molarity specimens indicated abundant hydroxyl ions in brucite and gypsum, which resulted in their poor performance against sulfate attack, while the shallow band in the higher-molarity specimens exhibited moderate sulfate resistance, and the unchanged transmittance intensity in the GBFS-free specimens exhibited significant resistance to sulfate attack.

6.5 Thermogravimetric analysis

The SiMnF and 30% GBFS incorporated alkali-activated composites were analyzed under thermogravimetric analysis, revealing four different phases of decomposition [63]. The first phase, between 32 ℃ and 105 ℃, was due to the evaporation of unbound water/activators, which was higher in control specimens and reduced by 78.5% in the GBFS mix. The second phase, between 110℃ and 380 ℃ due to the decomposition of hydration products, was observed to be 46% higher in GBFS than the control specimen. The third phase, between 380℃ and 460 ℃,

attributed to dehydroxylation of $Ca(OH)_2$ was 14% less in the GBFS mix than the control specimen, and the final phase, between 600℃ and 700 ℃, due to the carbonation, was reduced by 64% in the GBFS mix compared to the control mix. This indicated that higher chemically bound water/activators supported the condensation of oligomers in combination with a reduced carbonation in the GBFS incorporated mix, which enhanced its performance.

7 Durability properties

The durability aspects of SiMnF composites reported in the literature are discussed in this section. The resistance of alkali-activated SiMnF and GBFS composites against magnesium sulfate ($MgSO_4$) was evaluated by subjecting the specimens to a 5% $MgSO_4$ solution for 40 weeks (as shown in Fig. 11(a)) [61]. The GBFS-added high-alkaline binder showed the highest strength, reaching 49.4 MPa, and exhibited moderate stability against sulfate exposure. This was attributed to the enhanced microstructural densification and dissolution of source material (presumably silicomanganese compounds). In contrast, the GBFS-added mild-alkaline system achieved a moderate strength of 39.6 MPa but experienced progressive deterioration, mainly due to unreacted Ca^{2+} grains. The GBFS-free system had a maximum strength of 20.6 MPa, with relatively less damage due to the absence of sulfate phases and the formation of quartz, resulting from the lack of CaO in the composite.

Moreover, the resistance of these composites against sodium sulfate (Na_2SO_4) was also assessed by exposing the specimens to a 5% Na_2SO_4 solution for 40 weeks (as shown in Fig. 11(b)) [94]. The GBFS-blended high alkaline binder system demonstrated impressive sulfate resistance with an ultimate residual strength of 88.8% and minimal mass loss of 2.4%, attributed to a dense matrix of C-S–H, K-A-S–H, and C-Mn-H compounds. Conversely, the GBFS-blended mild-alkaline system displayed lower residual strength (74.1%) and increased mass loss (4.4%). Degradation under Na_2SO_4 exposure resulted from pH differentials, leading to additional gypsum and calcite formation due to ion mobility. Remarkably, the SiMnF system (i.e., without GBFS) displayed excellent stability under sulfate environments, attributed to the low calcium content in SiMnF. Figure 12 compares the sulfate performance of the SiMnF mixtures after 40 weeks of exposure to Na_2SO_4 and $MgSO_4$ [61, 94]. In this figure, three mixtures were examined: R(0)M(10), R(0.3)M(10), and R(0.3)M(4), where R(0) and R(0.3) denote the mass ratio of GBFS incorporation (either zero or 0.3), while M(10) and M(4) indicate high and low molarity of NaOH, respectively. Generally, magnesium sulfate is more aggressive than sodium sulfate. However, the incorporation of GBFS significantly improved strength development, with the high alkali system (10 M) demonstrating superior strength compared to the low alkali system (4 M).

Additionally, the sulfuric acid resistance of these composites was evaluated by subjecting them to a 5% H_2SO_4 acid solution for 20 weeks (as shown in Fig. 13) [98]. It was reported that the GBFS-free specimens showed high acid attack resistance due to the low calcium content in SiMnF, with a residual strength of 20.1%. The GBFS-mixed mild alkali system exhibited increased gypsum formation and dealumination, leading to severe spalling from incomplete Ca grain dissolution, resulting in a residual strength of 16%. In contrast, the GBFS-mixed high alkaline system displayed moderate resistance due to the dense microstructure formed by additional C-S–H, K-A-S–H, and C-Mn-H gel, enhancing retention of the polymerized framework, with a residual strength of 18.6%. Overall, the resistance of these composites against different sulfate and acid environments is influenced by various factors, including the composition ratios of Ca/Si, Ca/Mn, Si/Mn, Ca/K, and Si/K. Al-Duais et al. [99] developed alkali-activated concrete formulations by replacing 70%–90% of ordinary Portland cement (OPC) with various precursor materials. These included SiMnF (10%), limestone powder (10%), red mud (20%), and natural pozzolana (30%–50%), and their resistance against exposure to sulfuric acid (3%) and sulfate attack was evaluated. Remarkably, it was observed that alkali-activated concrete specimens with OPC content exceeding 10% exhibited resistance against both acid and sulfate attacks comparable to or even surpassing that of conventional OPC mixtures. This underscores the potential of incorporating alternative materials in alkali-activated concrete formulations to enhance their durability and environmental sustainability while maintaining or improving performance under harsh chemical exposures. Table 4 summarizes the details of the durability characteristics of SiMnF composites.

8 Sustainability assessment

Current methods for cement production raise many environmental concerns regarding the use of high energy in the production process, along with the process emissions, as well as the depletion of natural resources consumed in the formation of clinker. A recent report on the State of Climate Action 2023 [100] estimates that cement manufacturing contributes to 1.6 gigatonnes of CO_2-equivalent (Gt CO_{2e}) of the global net greenhouse gas (GHG) emissions, which accounts for around 13% of the industry's contribution. The 2020 estimates of the carbon footprint of global cement production were around 660 kg CO_2/t, while the 2030 target is 360–370 kg CO_2/t, as shown in Fig. 14. Thus, many efforts are required in the

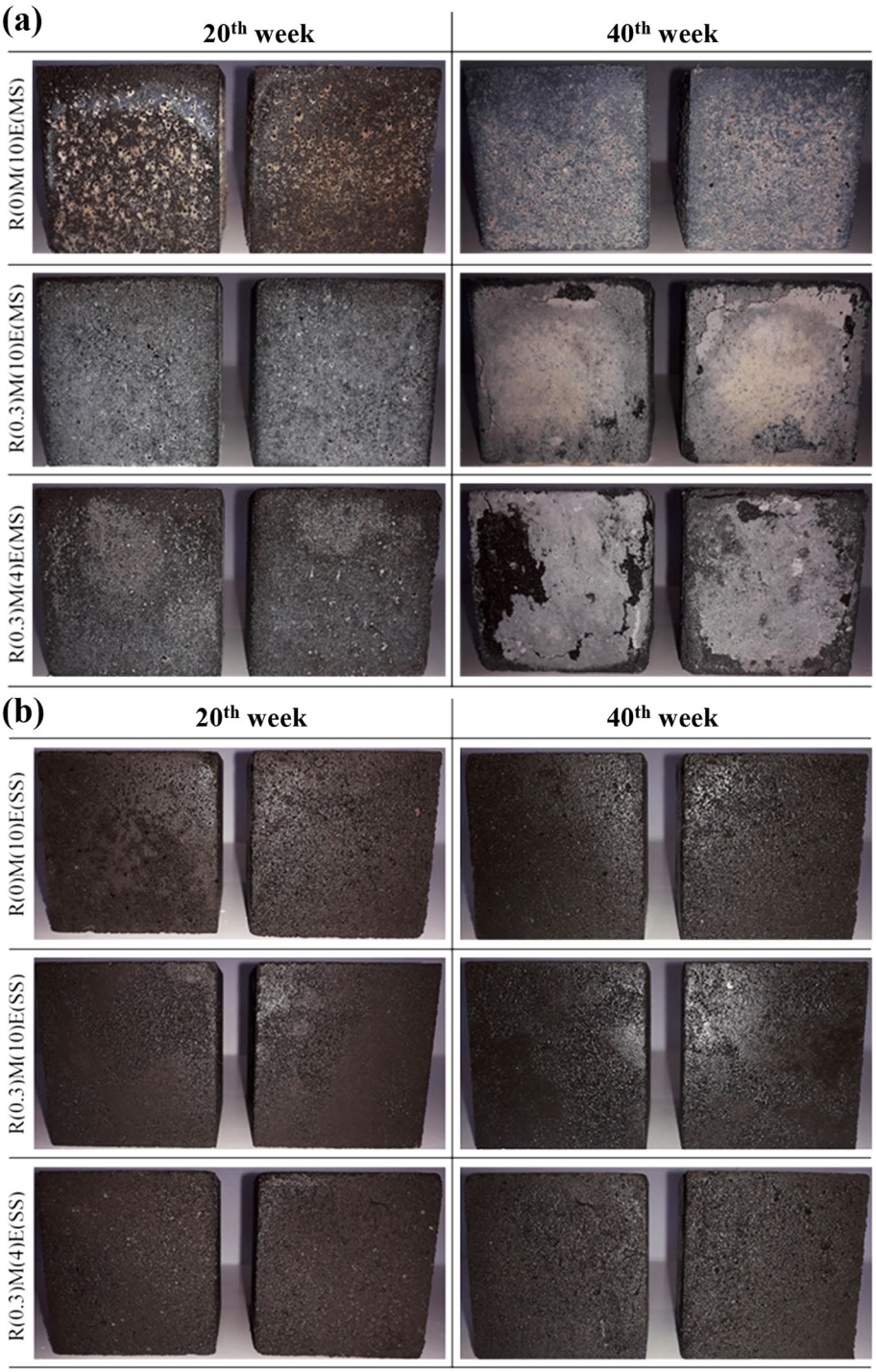

Fig. 11 Alkali-activated SiMnF specimens exposed to **a** 5% $MgSO_4$ solution, **b** 5% Na_2SO_4[61]

construction industry to reach the target, especially as infrastructure development demand is growing. Consequently, several materials and methods have been developed to mitigate the carbon footprint of cement production. Among these, the utilization of SCMs to replace the PC partially or fully is one of the most promising developments that can lower the emissions intensity in the short term [101]. As SiMnF is a by-product, or in many cases, a waste material, it can be classified as a low-carbon binder that can help reduce cement consumption.

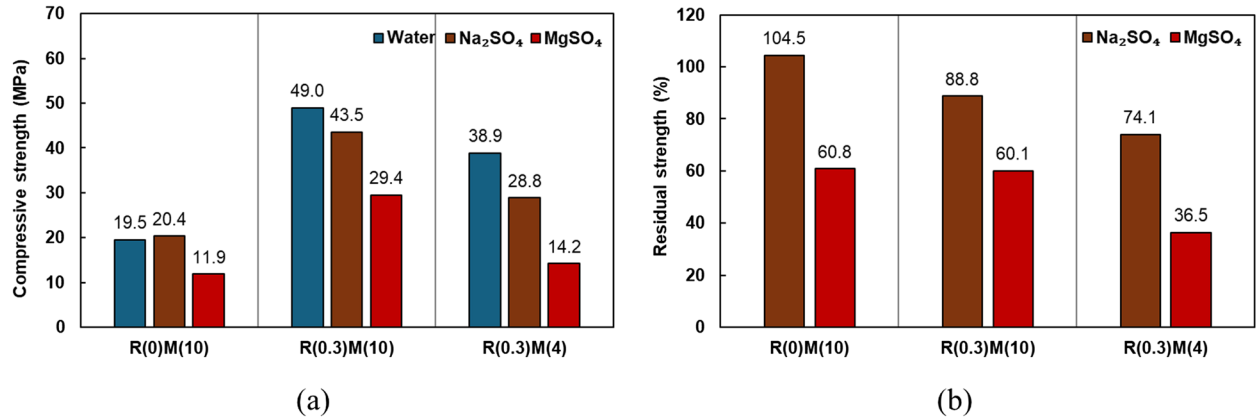

Fig. 12 Sulfate performance of the SiMnF mixtures after 40 weeks of exposure to Na_2SO_4 and $MgSO_4$ **a** Variation in the compressive strength. **b** Residual strength. [61, 94]

Such a sustainable alternative requires an environmental assessment to quantify its climate impact.

In this section, the ecological impact analysis of the SiMnF-based mixtures was evaluated using LCA. The analysis was conducted in accordance with the ISO 14040 standard [102], which defines the four main phases of LCA: (i) goal and scope definition, (ii) life cycle inventory (LCI), (iii) life cycle impact assessment (LCIA), and (iv) interpretation. The goal of this study was to assess the global warming potential (GWP) of concrete and mortar mixtures incorporating SiMnF. The functional unit was defined as 1 kg of produced mixes. The system boundaries followed a cradle-to-gate approach, which includes raw material extraction, processing, and transportation up to the production stage. Construction, use, and end-of-life stages were not considered. The LCA was quantified in the environmental indicator based on the equivalent CO_2 emissions (expressed as kg CO_2e/kg). Thus, the GWP of the mixtures' ingredients was obtained from the related literature [103–107]. To trade off between the environmental impact and the engineering performance, a mechanical-environmental indicator

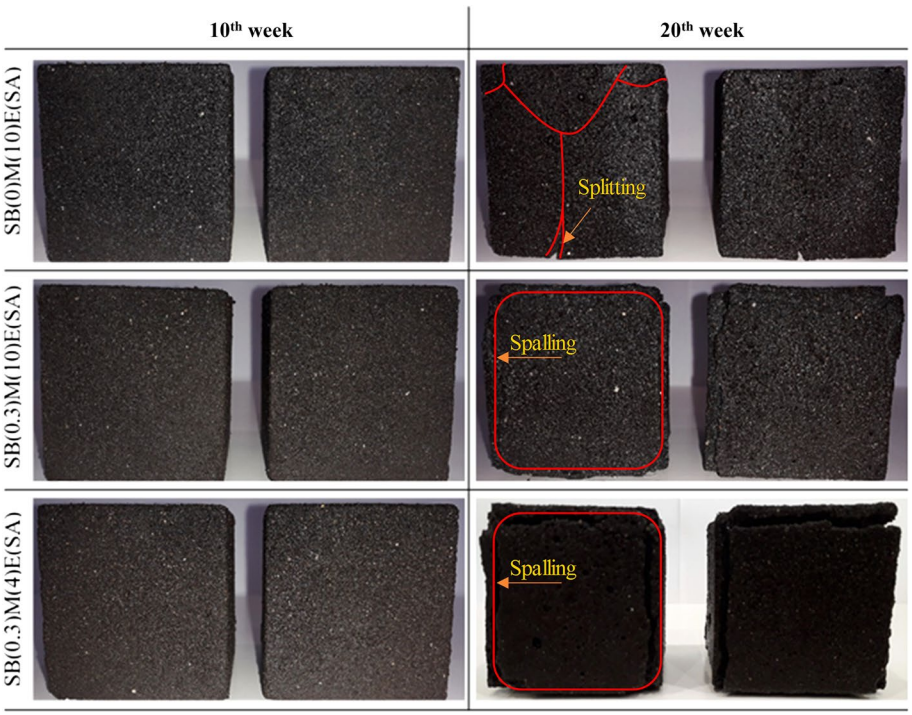

Fig. 13 Alkali-activated SiMnF specimens exposed to 5% sulfuric acid [98]

Table 4 Summary of the details of durability characteristics of SiMnF composites

Binder (%)	Key mix parameters investigated	Durability properties investigated	Exposure condition	Evaluation method	Durability performance	Ref.
SiMnF (100%–70%), GBFS (0–30%)	Impact of GBFS and molarity of NaOH (4 and 10 M)	Magnesium sulfate resistance	5% $MgSO_4$, 40 weeks	Physical appearance, mass loss, and residual strength	GBFS-free binder exhibited high resistance, GBFS-admixed high-alkaline binder exhibited moderate resistance, and GBFS-admixed mild-alkaline binder exhibited poor resistance to $MgSO_4$ attack	[61]
SiMnF (100%–70%), GBFS (0–30%)	Impact of GBFS and molarity of NaOH (4 and 10 M)	Sodium sulfate resistance	5% Na_2SO_4, 40 weeks	Visual inspection, mass loss, and residual strength	GBFS-free binder exhibited high resistance, GBFS-admixed high-alkaline binder exhibited moderate resistance, and GBFS-admixed mild-alkaline binder exhibited poor resistance to Na_2SO_4 attack	[94]
SiMnF (100%–70%), GBFS (0–30%)	Impact of GBFS and molarity of NaOH (4 and 10 M)	Sulfuric acid resistance	5% H_2SO_4, 20 weeks	Visual inspection, mass loss, and residual strength	GBFS-free binder exhibited high resistance, GBFS-admixed high-alkaline binder exhibited moderate resistance, and GBFS-admixed mild-alkaline binder exhibited poor resistance to H_2SO_4 attack	[98]

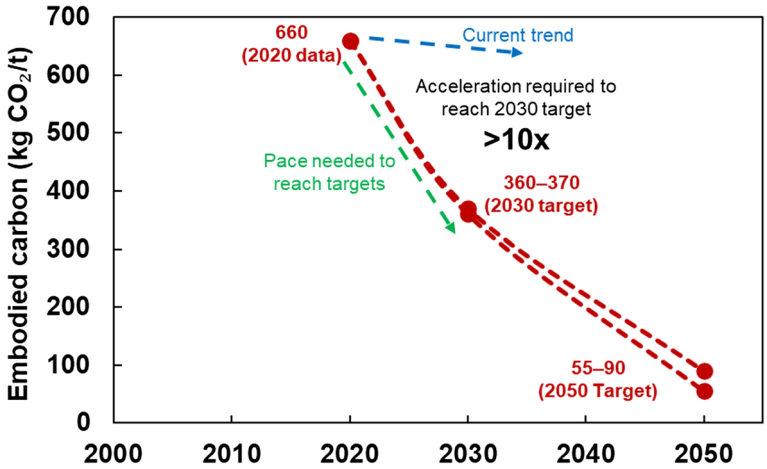

Fig. 14 Current and target carbon footprints of cement production (Reproduced from [100])

was used, which expresses the eco-strength index (I_{ES}). The I_{ES} was calculated as the ratio of the carbon footprint (in kg CO_2e) to the compressive strength (in MPa), thereby providing a metric that reflects both sustainability and structural performance, i.e., having a unit of kg CO_2e/MPa. Lower I_{ES} values indicate mixtures with better environmental-mechanical efficiency. As this study synthesizes LCA data from multiple published sources, no specific LCA software was employed; instead, comparative environmental indicators were computed based on standardized data sets and reported GWP values.

The environmental impact of the SiMnF mixtures has been studied in very limited research work. In a recent study [67], a detailed LCA analysis of the SiMnF mortars was conducted. The results revealed that the inclusion of higher proportions of SiMnF (>40%) reduced the CO_2 emissions by around 56% compared to 100% PC without any SCMs. In another study, Gawah et al. [64] conducted an elementary assessment of CO_2 emissions associated with self-compacting concrete, employing different proportions of SiMnF. The findings revealed a promising reduction in CO_2 emissions ranging from 10% to 68%, correlating with varying SiMnF content spanning from 10 to 70%. Despite these limited studies, a unified LCA-based comparison across all available mixtures is still lacking. Hence, this study compiles and analyzes the LCA results of different SiMnF-based mixes from the literature under a standardized framework to derive comparative insights.

Table 5 presents the proportions of the SiMnF-based mixes. A total of 39 mixes were included in this comparison study, predominantly consisting of alkali-activated mortars. Four binders were commonly blended in these mixes: SiMnF, GBFS, SF, and PC. In terms of alkaline activators, SS and SH were used in all alkali-activated mortars. It is worth mentioning that the carbon footprint of water was excluded in the LCA calculations as it had a negligible impact on the overall GWP. Mix M1 with 100% PC was included as a reference mortar for comparison. Figure 15 shows the embodied carbon results of all mixes. The range of CO_2 emissions of SiMnF-based mixtures was found to be between 0.060 and 0.182 kg CO_2/kg, while the reference mix without any SiMnF registered the highest emissions of 0.229 kg CO_2/kg. The LCA analysis revealed that the mix M5, having 100% SiMnF, had the lowest carbon footprint (0.060 kg CO_2/kg), highlighting the significant environmental impact of SiMnF. This corresponds to an emissions reduction of 74% compared to the reference mix. On the other hand, mix M38 blended with only 20% SiMnF showed a lower emissions reduction of around 20%.

Among the alkali-activated mixes (M2 through M31), the alkaline activators (SS and SH) were the major contributors to the total GWP. Thus, the activating chemicals were responsible for higher emissions as they are energy-intensive ingredients. This can also be shown in Fig. 16, which displays the breakdown of the CO_2 emissions. Typically, the SS and SH accounted for about 60% and 38%, respectively, of the total GWP. On the other mixes, M32 to M39, the presence of higher volumes of PC was the main reason for their emissions (i.e., PC accounted for over 99% of emissions in these mixes, as depicted in Fig. 16).

For more practical cases, it is essential to consider the engineering properties, such as compressive strength, along with the environmental aspects. Thus, the strength-normalized index, called the eco-strength index (I_{ES}) indicator, was evaluated. Figure 17(a) depicts the CO_2 emissions of SiMnF-based mixes with their associated compressive strength. Generally, CO_2 emissions followed the trend of compressive strength, implying that the use of more intensive carbon ingredients leads to increased

Table 5 Proportions of the SiMnF-based mixes included in the LCA study

Mix No.	Mix proportions (kg/m^3)							Ref.
	OPC	SiMnF	GBFS	SF	Sand	SS	SH	
M1	797.8	0	0	0	1196.7	0	0	[67]
M2	0	470.0	0	0	940.0	134.7	67.4	[80]
M3	0	470.0	0	0	940.0	144.3	57.7	[80]
M4	0	470.0	0	0	940.0	151.6	50.52	[80]
M5	0	723.0	0	0	1301.4	0	103.2	[62]
M6	0	723.0	0	0	1301.4	180.6	180.6	[62]
M7	0	723.0	0	0	1301.4	216.7	144.5	[62]
M8	0	723.0	0	0	1301.4	240.8	120.4	[62]
M9	0	723.0	0	0	1301.4	258.0	103.2	[62]
M10	0	723.0	0	0	1301.4	270.9	90.3	[62]
M11	0	723.0	0	0	1301.4	280.9	80.3	[62]
M12	0	723.0	0	0	1084.5	241.0	120.5	[90]
M13	0	723.0	0	0	1301.4	263.4	105.3	[90]
M14	0	723.0	0	0	1301.4	258	103.2	[92]
M15	0	723.0	0	0	1735.2	298.0	85.1	[90]
M16	0	723.0	0	0	1518.3	282.0	94.0	[90]
M17	0	650.7	72.3	0	1301.4	258	103.2	[92]
M18	0	578.4	144.6	0	1301.4	258	103.2	[92]
M19	0	506.1	216.9	0	1301.4	258	103.2	[92]
M20	0	397.6	325.3	0	1084.5	268.54	107.4	[90]
M21	0	614.5	108.4	0	1735.2	258.2	103.3	[90]
M22	0	397.6	325.3	0	1518.3	281.2	80.3	[90]
M23	0	506.1	216.9	0	1518.3	273.7	109.5	[90]
M24	0	397.6	325.3	0	1301.4	255.5	127.7	[90]
M25	0	614.5	108.4	0	1084.5	287.4	95.8	[90]
M26	0	506.1	216.9	0	1084.5	286.8	81.94	[90]
M27	0	614.55	108.45	0	1301.4	292.41	83.55	[90]
M28	0	397.65	325.35	0	1735.2	276.55	92.18	[90]
M29	0	614.55	108.45	0	1518.3	245.82	122.91	[90]
M30	0	506.1	216.9	0	1301.4	271.13	90.38	[90]
M31	0	506.1	216.9	0	1735.2	250.64	125.32	[90]
M32	514.5	128.6	0	0	1286.2	0	0	[67]
M33	401.1	291.7	0	36.4	1094	0	0	[67]
M34	339.7	271.8	0	67.9	1359.1	0	0	[67]
M35	351.6	234.4	0	0	1465	0	0	[67]
M36	453	120.8	0	30.2	1510.1	0	0	[67]
M37	530.2	151.5	0	75.7	1136.3	0	0	[67]
M38	635.1	158.7	0	0	1190.8	0	0	[67]
M39	592.9	158.1	0	39.5	1185.9	0	0	[67]

strength (Fig. 17(a)). But how to assess this reduction in strength? Fig. 17(b) provides some insights by presenting the calculated I_{ES} indicator, which is a combined index.

It was found that mix M34 with 40% SiMnF exhibited the lowest I_{ES} value (2.6×10^{-3} kg CO_2e/MPa) as it had a good compressive strength of 38 MPa and low emissions of 0.098 kg CO_2/kg. However, mix M19 registered the highest I_{ES} value (7.29×10^{-3} kg CO_2e/MPa) due to its lower compressive strength (19.0 MPa) and relatively higher emissions (2.554 kg CO_2/kg). Therefore, the LCA comparison results revealed that a viable and promising environmental impact can be achieved through optimizing the mix proportions with low-carbon ingredients. This suggests that SiMnF can be utilized as a low-carbon binder for producing sustainable mixtures having reasonably acceptable compressive strength.

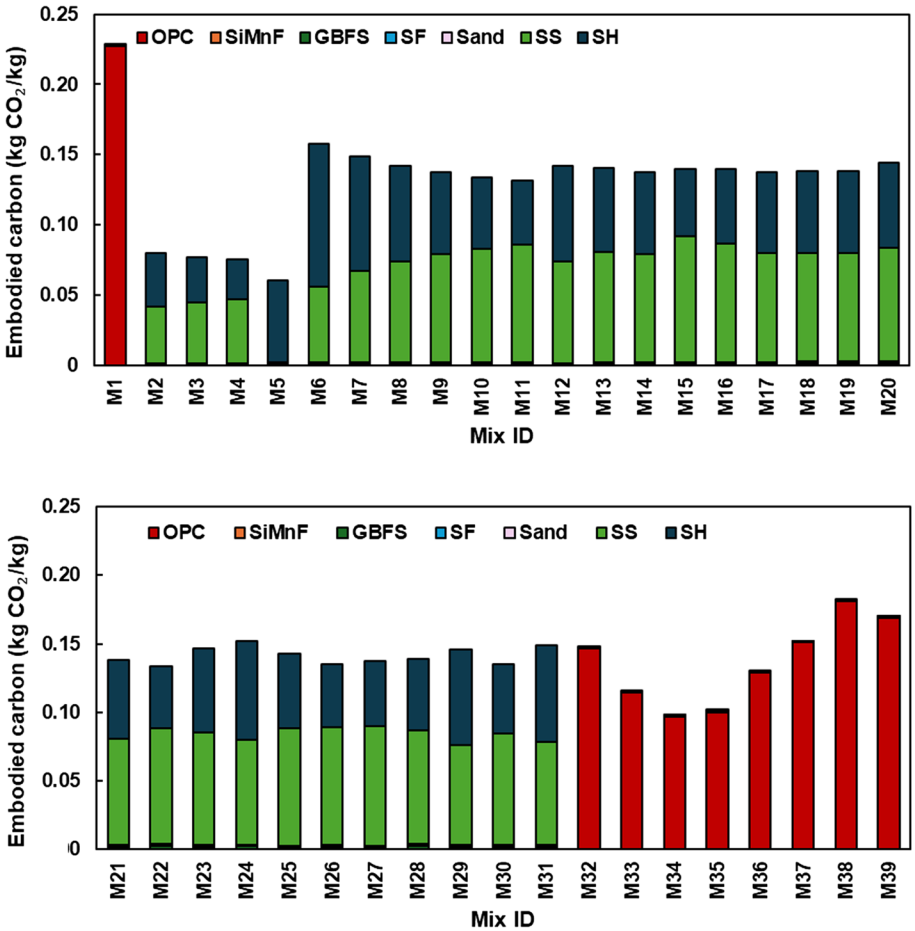

Fig. 15 LCA analysis: embodied carbon of SiMnF-based mixes

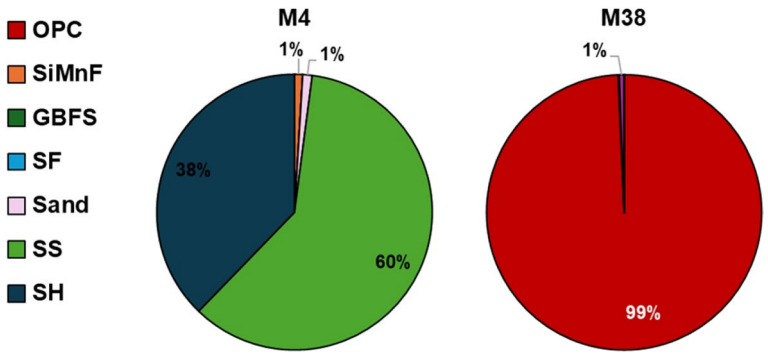

Fig. 16 CO_2 emissions breakdown of SiMnF-based mixes

9 Challenges and future perspectives

The use of SiMnF as a construction material presents a promising substitute for conventional materials such as cement and other value-added, expensive, or often imported SCMs, such as slag, FA, and SF, whose declining production and increasing demand are concerning. Despite the potential for the use of SiMnF as an alternative SCM, certain challenges need to be addressed when incorporating SiMnF into infrastructural applications. Therefore, this section highlights the knowledge gaps and research priorities crucial for promoting and upscaling the SiMnF-based binders.

The integration of design of experiments (DoE) methods and optimization statistical techniques in the SiMnF

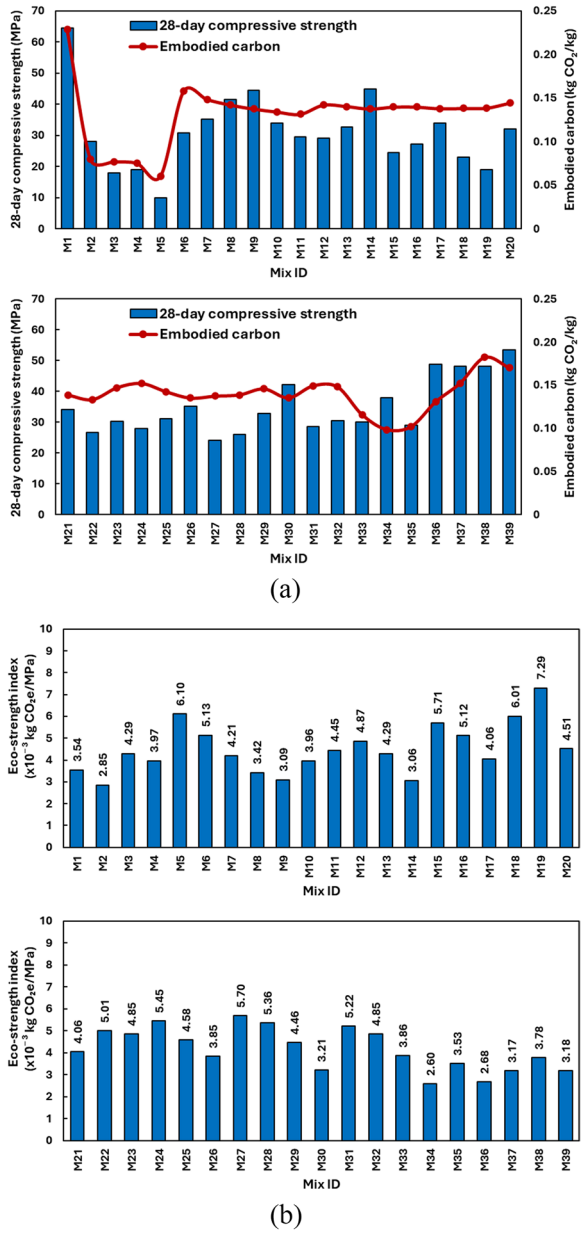

Fig. 17 Sustainability assessment. **a** CO_2 emissions of SiMnF-based mixes with their associated compressive strength. **b** Eco-strength efficiency of SiMnF-based mixes

mixtures holds significant importance. These approaches offer a systematic approach for formulating and enhancing concrete compositions, offering advantages over traditional trial-and-error approaches. One prominent DoE method is the Taguchi method (TM), widely recognized for its efficacy in minimizing the need for intensive experimental iterations [90]. In addition, optimization methods, such as the response surface approach, can be effectively employed to optimize mixtures, achieving desired engineering properties while considering economic and sustainability factors. Therefore, the design of a SiMnF-based concrete mixture should incorporate statistical methods.

Literature lacks quantified economic viability of SiMnF as a construction material, simply because most end up in landfilling and stockpiling; instances where it is used as an SCM or a cement blend remain a regulated trade secret. The associated costs can still be traced to safe handling, storing, and transporting to cement plants. This review paper notes that SiMnF does not require further processing and grinding to be blended with cement to offset clinkers, and as such, this byproduct can offset the costs of cement production. If SiMnF can be sourced locally and handled cost-effectively, competitive production of SiMnF-blended cement is possible. However, it is anticipated that just like FA and GBFS, with a progressively higher demand, the price of SiMnF can be expected to rise close to the unit price of Portland cement eventually. Nonetheless, a more durable product ensures lower rates of maintenance and replacements, offering longer service life at a cost-saving.

The literature survey reveals that most reported mechanical properties of alkali-activated SiMnF-based mixtures are basic, primarily focusing on compressive strength evaluation. Detailed mechanical performance, for possible structural applications, including the tensile and flexural strengths as well as modulus of elasticity, is yet to be investigated. In addition, the existing literature primarily pertains to mortar mixtures, neglecting concrete-related properties involving coarse aggregates. The compatibility of SiMnF with other constituents of concrete and mortar, such as aggregates and admixtures, needs to be thoroughly evaluated to prevent undesirable interactions and ensure structural performance.

Literature lacks comprehensive data on the durability characteristics of SiMnF-based mixtures. Especially, studies on permeability, water absorption, pore size distribution, chloride diffusion, reinforcement corrosion, alkali-silica reaction, freeze–thaw resistance, abrasion resistance, performance under elevated temperatures, and fire resistance are needed. In addition, dimensional stability, including plastic shrinkage, drying shrinkage, creep, and thermal expansion, requires evaluation. Besides, the long-term durability performance under various environmental conditions is yet to be explored to monitor the resilience of SiMnF in concrete over time, ensuring durable structures.

Most developed SiMnF-based mixtures are alkali-activated composites, where alkali activators, such as SS and SH, contribute significantly to environmental impact due to their energy intensity and carbon footprints. Optimization of mixture designs should aim to minimize

activator content where possible. Exploring alternative alkaline activators stemming from natural resources holds promise for reducing environmental impact. On the other hand, heat curing is occasionally used to activate binder-based mixtures but raises production costs and environmental concerns due to energy intensity. Therefore, promoting room-temperature curing methods for developing sustainable mixtures is essential. Besides the effects of curing temperature and duration, the relative humidity can be investigated to optimize the most efficient curing regime suitable for the SiMnF mixtures [93]. In this way, the possibility of cast-in-place SiMnF-based concrete could be upscaled into real applications.

While GWP was selected as the primary environmental indicator in this study due to its relevance to climate-related impacts and the availability of consistent data, other important categories, such as acidification, eutrophication, resource depletion, and water scarcity, were not included because of limited or inconsistent reporting across the reviewed studies. Future research should aim to incorporate these additional indicators for a more comprehensive sustainability assessment of SiMnF-based mixtures. In addition to the eco-strength index used in this study, more comprehensive eco-mechanical evaluation methods have been proposed in the literature for SCMs. For example, the recent work by Sirico et al. [108] introduces a multi-criteria framework, in which combining splitting tensile strength and ductility could be considered in future studies to develop a more integrated assessment of SiMnF-based systems.

Future research prospects for SiMnF-based mixtures include the utilization of nanomaterials (to enhance the material properties) and the incorporation of by-products from other industries (to enhance quality and sustainability). Given SiMnF's low Ca and high Mn and K content [94], using Ca-rich materials can significantly enhance reactivity and improve mechanical strength. While some SiMnF-based mixtures show promising strength characteristics, further research is needed on their flexural and shear behavior in structural elements such as beams, columns, and slabs. These studies can lead to the development of design guidelines and construction codes tailored for SiMnF-based concrete, facilitating its broader acceptance in the construction industry. Current construction standards, which are often prescriptive rather than performance-based, may pose challenges to integrating new materials such as low-carbon binders in practical applications. Overcoming these challenges is essential to realizing the potential benefits of alternative materials in sustainable construction practices. To that extent, it is to be noted that in using SiMnF, there are some health concerns handling the material (as with any dust, including cement) that need mentioning as a future challenge to the adaptation of this as an SCM. It is recommended that SiMnF collection and delivery to concrete plants follow stringent procedures to eliminate dust exposure. A more severe issue is possibly a lack of understanding of leachates from SiMnF concrete run-offs and pore extracts. Future research should address the critical gap in understanding the leaching behavior of SiMnF-based mixes, particularly under varied exposure conditions. This includes investigating the pore solution for unbound heavy metal ions and assessing their mobilization through leaching experiments to identify potential environmental risks.

10 Conclusions

SiMnF, a by-product of the ferroalloy industry, holds remarkable potential for use in the construction industry. This review examines the synthesis, reaction mechanisms, and evaluation of the engineering properties of alkali-activated SiMnF-based mixtures. A comprehensive ecological impact analysis of the SiMnF-based mixtures was conducted using LCA. Despite progress in research, many aspects of SiMnF-based mixtures remain unexplored, including detailed mechanical performance, concrete-related properties, and long-term durability characteristics. Based on the research findings and LCA, the following points are highlighted:

- SiMnF possesses desirable physical properties such as a reasonable particle size (D_{50} = 29.17 μm), which offers a good packing effect and density. Its spherical texture can improve workability due to the ball-bearing effect, enabling its application in self-compacting concrete. However, its composition, primarily MnO, SiO_2, and K_2O (over 70%), with a dearth of CaO (7.24%) and Al_2O_3 (1.46%), results in poor reactivity and a low rate of strength development.
- SiMnF is primarily used in alkali-activated composites and self-compacting concrete. Common activators include NaOH and Na_2SiO_3, with NaOH concentrations ranging from 2.5 to 16 M and alkali activator ratios from 1 to 3.5. Some studies utilized the Taguchi method for optimizing their mix designs due to various key parameters.
- Mechanical properties of SiMnF-based materials are rarely investigated beyond compressive strength. In self-compacting concrete, mechanical properties decline as SiMnF content exceeds 20%. For alkali-activated SiMnF mortars, strengths of 45–50 MPa are achievable at optimal NaOH molarity (10 M) and alkaline activator ratio (2.5). Heat curing at 60 ℃ for 6 h yields 83.5% of the 28-day strength in just 3 days.
- The microstructure of alkali-activated SiMnF mortar improves at higher NaOH molarity owing to

greater polymerization, resulting in a compact matrix with fewer pores. Elemental composition and XRD analysis revealed the formation of Mn-S–H type gel as a reaction product at higher alkali activator concentrations. These microstructural changes correlate well with improved mechanical properties and resistance to acid or sulfate attacks.
- Limited studies on sulfate resistance in $MgSO_4$ and Na_2SO_4 solutions for 40 weeks showed good performance due to the absence of sulfate phases and formation of quartz, attributed to the low CaO content.
- Environmental assessments, in terms of life-cycle analysis, classify SiMnF as a low-carbon binder, capable of reducing CO_2 emissions by up to 40% in alkali-activated mixtures compared to 100% OPC mixtures with similar strength grades. However, alkaline activators significantly contribute to the total carbon footprint of alkali-activated SiMnF mixtures. Therefore, the carbon reduction can be as high as 60% in standard SiMnF-based mortar mixtures.
- Blending SiMnF-based composites with SF or blast furnace slag can densify the microstructure and enhance mechanical and durability properties, although this may reduce flow and setting times.

Authors' contributions

Muhammad Nasir: Conceptualization, Methodology, Investigation, Data Curation, Writing–Original Draft, Writing–Review & Editing, Visualization, Project Administration. Ashraf A. Bahraq: Conceptualization, Methodology, Investigation, Data Curation, Writing– Original Draft, Writing–Review & Editing, Visualization. Rida Assaggaf: Methodology, Investigation, Data Curation, Writing–Original Draft, Writing–Review & Editing. Shaik Inayath Basha: Validation, Investigation, Data Curation, Writing–Original Draft, Writing–Review & Editing, Visualization. Aziz Hasan Mahmood: Investigation, Writing–Original Draft, Writing–Review & Editing.

Funding

This research received no specific grant from any funding agency in the public, commercial, or not-for-profit sectors.

Data availability

The datasets generated and/or analyzed during the current study are available from the corresponding author on reasonable request.

Declarations

Competing interests

The authors declare that there are no financial or non-financial interests that are directly or indirectly related to the work submitted for publication.

Author details

[1]ReSET Group, Physical Sciences and Engineering (PSE) Division, Clean Energy Research Platform, King Abdullah University of Science and Technology (KAUST), Thuwal, Saudi Arabia. [2]Interdisciplinary Research Center for Construction and Building Materials, King Fahd University of Petroleum & Minerals, 31261 Dhahran, Saudi Arabia. [3]Applied Research Center for Metrology, Standards and Testing, King Fahd University of Petroleum & Minerals, 31261 Dhahran, Saudi Arabia. [4]School of Civil and Environmental Engineering, University of Technology Sydney, Broadway, NSW 2007, Australia.

Received: 20 June 2025 Revised: 23 August 2025 Accepted: 22 September 2025
Published: 27 November 2025

References

1. Scrivener, K. L., John, V. M., & Gartner, E. M. (2018). Eco-efficient cements: Potential economically viable solutions for a low-CO_2 cement-based materials industry. *Cement and Concrete Research, 114*, 2–26. https://doi.org/10.1016/j.cemconres.2018.03.015
2. Boesch, M. E., Koehler, A., & Hellweg, S. (2009). Model for cradle-to-gate life cycle assessment of clinker production. *Environmental Science & Technology, 43*, 7578–7583. https://doi.org/10.1021/es900036e
3. Singh, G. V. P. B., & Subramaniam, K. V. L. (2019). Production and characterization of low-energy Portland composite cement from post-industrial waste. *Journal of Cleaner Production, 239*, Article 118024. https://doi.org/10.1016/j.jclepro.2019.118024
4. Nidheesh, P. V., & Kumar, M. S. (2019). An overview of environmental sustainability in cement and steel production. *Journal of Cleaner Production, 231*, 856–871. https://doi.org/10.1016/j.jclepro.2019.05.251
5. Ahmad, W., Ahmad, A., Ostrowski, K. A., Aslam, F., & Joyklad, P. (2021). A scientometric review of waste material utilization in concrete for sustainable construction. *Case Studies in Construction Materials, 15*, Article e00683.
6. Sandanayake, M., Bouras, Y., Haigh, R., & Vrcelj, Z. (2020). Current sustainable trends of using waste materials in concrete—A decade review. *Sustainability, 12*, 9622.
7. Estrellan, C. R., & Iino, F. (2010). Toxic emissions from open burning. *Chemosphere, 80*, 193–207. https://doi.org/10.1016/j.chemosphere.2010.03.057
8. He, C., Yu, R., Chen, Z., & Sun, H. (2016). Research on unattended hoisting in solid waste disposal. *International Journal of Hydrogen Energy, 41*, 15817–15820. https://doi.org/10.1016/j.ijhydene.2016.04.185
9. Bartelings, H., van Beukering, P., Kuik, O., Linderhof, V., Oosterhuis, F., Brander, L., & Wagtendonk, A. (2005). *Effectiveness of landfill taxation, report prepared for the Dutch Ministry of Housing, spatial planning and the environment*. Vrije Univ.
10. Basha, S. I., Ali, M. R., Al-Dulaijan, S. U., & Maslehuddin, M. (2020). Mechanical and thermal properties of lightweight recycled plastic aggregate concrete. *Journal of Building Engineering, 32*, Article 101710.
11. Basha, S. I., Ali, M. R., Shameem, M., Al-Dulaijan, S. U., & Maslehuddin, M. (2023). Durability of recycled waste plastic aggregate concrete. *European Journal of Environmental and Civil Engineering, 27*, 663–684.
12. Aprianti, E., Shafigh, P., Bahri, S., & Farahani, J. N. (2015). Supplementary cementitious materials origin from agricultural wastes–a review. *Construction and Building Materials, 74*, 176–187. https://doi.org/10.1016/j.conbuildmat.2014.10.010
13. Buchwald, A., & Schulz, M. (2005). Alkali-activated binders by use of industrial by-products. *Cement and Concrete Research, 35*, 968–973. https://doi.org/10.1016/j.cemconres.2004.06.019
14. Nasir, M., Al-Amoudi, O. S. B., Al-Gahtani, H. J., & Maslehuddin, M. (2016). Effect of casting temperature on strength and density of plain and blended cement concretes prepared and cured under hot weather conditions. *Construction and Building Materials, 112*, 529–537. https://doi.org/10.1016/j.conbuildmat.2016.02.211
15. Zhan, P., He, Z., Ma, Z., Liang, C., Zhang, X., Abreham, A. A., & Shi, J. (2020). Utilization of nano-metakaolin in concrete: A review. *Journal of Building Engineering, 30*, Article 101259.
16. Mousavinezhad S., Gonzales G. J., Toledo W. K., Garcia J. M., Newtson C. M. (2022). Mechanical Properties of Ultra-High-Performance Concrete Containing Natural Pozzolan and Metakaolin. In *Tran-SET 2022* (pp. 200–208).
17. Kadhim, A., Sadique, M., Al-Mufti, R., & Hashim, K. (2021). Developing one-part alkali-activated metakaolin/natural pozzolan binders using lime waste. *Advances In Cement Research, 33*, 342–356.

18. Ahmad, S., Bahraq, A. A., Shaqraa, A. A., Khalid, H. R., Al-Gadhib, A. H., & Maslehuddin, M. (2022). Effects of key factors on the compressive strength of metakaolin and limestone powder-based alkali-activated concrete mixtures: An experimental and statistical study. *Case Studies in Construction Materials, 16*, Article e00915. https://doi.org/10.1016/j.cscm.2022.e00915
19. Al-Fakih, A., Mohamed Nor, Z., Inayath Basha, S., Nasiruzzaman Shaikh, M., Ahmad, S., Al-Osta, M. A., & Aziz, M. A. (2023). Characterization and applications of red mud, an aluminum industry waste material, in the construction and building industries, as well as catalysis. *Chemistry Record, 23*, Article e202300039.
20. M. Tangstad. (2013). Manganese Ferroalloys Technology. In Handb. *Ferroalloys Theory Technol* (pp. 221–266). Elsevier. https://doi.org/10.1016/B978-0-08-097753-9.00007-1.
21. Ibrahim, M., Maslehuddin, M., Khallaf, Z. A., Joseph, J. J. I., & Mamilla, S. B. (2025). Brine sludge activated ground volcanic pumice-based alkali activated binder. *Construction and Building Materials*, *483*, 141836.
22. Lan, J., Dong, Y., Kai, M.-F., Hou, H., & Dai, J.-G. (2024). Investigation of waste alkali-activated cementing material using municipal solid waste incineration fly ash and dravite as precursors: Mechanisms, performance, and on-site application. *Journal Of Hazardous Materials, 465*, Article 133416.
23. Nasir, M., Mahmood, A. H., & Bahraq, A. A. (2024). History, recent progress, and future challenges of alkali-activated binders–An overview. *Construction and Building Materials, 426*, Article 136141.
24. Provis, J. L. (2018). Alkali-activated materials. *Cement and Concrete Research, 114*, 40–48. https://doi.org/10.1016/j.cemconres.2017.02.009
25. Singh, J., & Singh, S. P. (2019). Geopolymerization of solid waste of non-ferrous metallurgy – A review. *Journal Of Environmental Management, 251*, Article 109571.
26. International Manganese Institute (IMnI). *Annual Review*. (2021). https://www.manganese.org/sites/default/files/featured_images/2021-Annual-Review-EN.pdf.
27. Singh, V., Chakraborty, T., & Tripathy, S. K. (2020). A review of low grade manganese ore upgradation processes. *Mineral Processing and Extractive Metallurgy Review, 41*, 417–438.
28. Hernandez-Pellón, A., Fernandez-Olmo, I., Ledoux, F., Courcot, L., & Courcot, D. (2017). Characterization of manganese-bearing particles in the vicinities of a manganese alloy plant. *Chemosphere, 175*, 411–424. https://doi.org/10.1016/j.chemosphere.2017.02.056
29. Rai, A., Prabakar, J., Raju, C. B., & Morchalle, R. K. (2002). Metallurgical slag as a component in blended cement. *Construction and Building Materials, 16*, 489–494. https://doi.org/10.1016/S0950-0618(02)00046-6
30. S.A.K. Thomas K. (2014). Market Survey on Manganese Ore. *Indian Bur. Mines*, *235*.
31. Ma, Y., Moosavi-Khoonsari, E., Kero, I. T., & Tranell, G. M. (2018). Element distribution in the silicomanganese production process. *Metallurgical And Materials Transactions B, 49*, 2444–2457. https://doi.org/10.1007/s11663-018-1358-9
32. Santamaria, A. B. (2008). Manganese exposure, essentiality & toxicity. *Indian Journal of Medical Research, 128*, 484.
33. Freeland-Graves J.H., Mousa T.Y., Sanjeevi N. (2015). Nutritional requirements for manganese. In Lucio C., & Michael A. (Eds.), *Health and Disease* (pp. 34–75). Royal Society of Chemistry. https://doi.org/10.1039/9781782622383-00034.
34. Keen, C. L., Ensunsa, J. L., & Clegg, M. S. (2000). Manganese metabolism in animals and humans including the toxicity of manganese. *Metal Ions in Biological Systems, 37*, 89–121. https://doi.org/10.1201/9781482289893-14
35. ATSDR (2012, September). *A toxicological profile for manganese.* Retrieved October 2024, from https://www.atsdr.cdc.gov/toxprofiles/tp151.pdf
36. WHO. (2000). Air Quality Guidelines for Europe. World Health Organization Regional Publications, European Series, No. 91. Retrieved October 2024, from https://apps.who.int/iris/handle/10665/ 107335.
37. Flynn, M. R., & Susi, P. (2009). Neurological risks associated with manganese exposure from welding operations - A literature review. *International Journal of Hygiene and Environmental Health, 212*, 459–469. https://doi.org/10.1016/j.ijheh.2008.12.003
38. Park, R. M. (2013). Neurobehavioral deficits and parkinsonism in occupations with manganese exposure: A review of methodological issues in the epidemiological literature. *Safety and Health at Work, 4*, 123–135. https://doi.org/10.1016/j.shaw.2013.07.003
39. Kwakye, G. F., Paoliello, M. M. B., Mukhopadhyay, S., Bowman, A. B., & Aschner, M. (2015). Manganese-induced parkinsonism and Parkinson's disease: Shared and distinguishable features. *International Journal of Environmental Research and Public Health, 12*, 7519–7540. https://doi.org/10.3390/ijerph120707519
40. U.S. Department of Health and Human Services, Public Health Service. (2003). *Toxicological profile for pyrethrins and pyrethroids.* Agency for Toxic Substances and Disease Registry.
41. Williams, M., Todd, G. D., Roney, N., Crawford, J., Coles, C., McClure, P. R., Garey, J. D., Zaccaria, K., & Citra, M. (2012). *Toxicological Profile for Manganese.* Agency for Toxic Substances and Disease Registry (US), Atlanta (GA).
42. Haynes, E. N., Heckel, P., Ryan, P., Roda, S., Leung, Y. K., Sebastian, K., & Succop, P. (2010). Environmental manganese exposure in residents living near a ferromanganese refinery in Southeast Ohio: A pilot study. *Neurotoxicology, 31*, 468–474. https://doi.org/10.1016/j.neuro.2009.10.011
43. Ledoux, F., Laversin, H., Courcot, D., Courcot, L., Zhilinskaya, E. A., Puskaric, E., & Aboukaïs, A. (2006). Characterization of iron and manganese species in atmospheric aerosols from anthropogenic sources. *Atmospheric Research, 82*, 622–632. https://doi.org/10.1016/j.atmosres.2006.02.018
44. Querol, X., Viana, M., Alastuey, A., Amato, F., Moreno, T., Castillo, S., Pey, J., de la Rosa, J., Sánchez de la Campa, A., Artíñano, B., Salvador, P., García Dos Santos, S., Fernández-Patier, R., Moreno-Grau, S., Negral, L., Minguillón, M. C., Monfort, E., Gil, J. I., Inza, A., … Zabalza, J. (2007). Source origin of trace elements in PM from regional background, urban and industrial sites of Spain. *Atmospheric Environment, 41*, 7219–7231. https://doi.org/10.1016/j.atmosenv.2007.05.022
45. Moreno, T., Pandolfi, M., Querol, X., Lavín, J., Alastuey, A., Viana, M., & Gibbons, W. (2011). Manganese in the urban atmosphere: Identifying anomalous concentrations and sources. *Environmental Science And Pollution Research, 18*, 173–183. https://doi.org/10.1007/s11356-010-0353-8
46. CIMA. (2006). *Evaluation of the influence of wind direction on Manganese Content of PM10 collected in Alto de Maliaño*. Government of Cantabria, Internal report C-098/2004.4, Retrieved August 2023 from https://repositorio.unican.es/xmlui/bitstream/handle/10902/16236/TESIS%20AMHP.pdf?sequence=1&isAllowed=y
47. CIMA. (2010). *Air quality evaluation and metal analysis of the PM10 fraction in Alto de Maliaño*. Government of Cantabria, Internal report C-077/2008, Retrieved August 2023 from https://repositorio.unican.es/xmlui/bitstream/handle/10902/16236/TESIS%20AMHP.pdf?sequence=1&isAllowed=y
48. Arruti, A., Fernández-Olmo, I., & Irabien, Á. (2010). Evaluation of the contribution of local sources to trace metals levels in urban PM2.5 and PM10 in the Cantabria region (northern Spain). *Journal of Environmental Monitoring, 12*, 1451–1458. https://doi.org/10.1039/b926740a
49. Ruiz, S., Fernández-Olmo, I., & Irabien, Á. (2014). Discussion on graphical methods to identify point sources from wind and particulate matter-bound metal data. *Urban Climate, 10*, 671–681. https://doi.org/10.1016/j.uclim.2013.11.001
50. Hernández-Pellón, A., & Fernández-Olmo, I. (2016). Monitoring the levels of particle matter-bound manganese: An intensive campaign in an urban/industrial area. *2nd International Conference on Atmospheric Dust - DUST2016.* ProScience. https://doi.org/10.14644/dust.2016.008.
51. Safarian, J. (2022). A sustainable process to produce manganese and its alloys through hydrogen and aluminothermic reduction. *Processes, 10*, 27. https://doi.org/10.3390/pr10010027
52. Randhawa, N. S., Minj, R. K., & Kumar, K. (2024). Eco-friendly low-carbon manganese ferroalloy production for cleaner steel technologies. *Clean Technologies and Environmental Policy, 21*, Article 100784. https://doi.org/10.1016/j.clet.2024.100784
53. Wong, N. H., Kong, Z. Y., Sambo, R., Chai, C. S., Khoso, A. R., Bamgbade, J. A., & Sunarso, J. (2024). Physicochemical Characteristics of Silicomanganese Slag as a Recycling Construction Material: An Overview, Mining. *Metall. Explor., 41*, 1891–1907. https://doi.org/10.1007/s42461-024-00987-3

54. Godbole, P., Meshram, P., Jawadand, S., Meshram, T., & Randive, K. (2025). A critical analysis of industrial slags, their hazard potential and remediation with reference to Sustainable Development Goals (SDGs). *Discover Civil Engineering, 2*, 117. https://doi.org/10.1007/s44290-025-00242-8
55. Zhang, S., Yao, J., Wu, P., Feng, X., Ban, J., Zhang, S., Sunahara, G., & Ni, W. (2024). A low-carbon cement based on silicomanganese slag and granulated blast furnace slag: Hydration process, microstructure, mechanical properties and leaching risks. *Journal Of Building Engineering, 94*, Article 109939. https://doi.org/10.1016/j.jobe.2024.109939
56. Nath, S. K., Randhawa, N. S., & Kumar, S. (2022). A review on characteristics of silico-manganese slag and its utilization into construction materials. *Resources, Conservation and Recycling, 176*, Article 105946. https://doi.org/10.1016/j.resconrec.2021.105946
57. Małecki, S., Gargul, K., Warzecha, M., Stradomski, G., Hutny, A., Madej, M., Dobrzyński, M., Prajsnar, R., & Krawiec, G. (2021). High-performance method of recovery of metals from eaf dust—processing without solid waste. *Materials, 14*, Article 6061. https://doi.org/10.3390/ma14206061
58. Rashid, S., Khalid, H. R., & Hanif, A. (2025). Mechanical behavior and leaching characteristics of cementitious composites incorporating silicomanganese fume. *European Journal of Environmental and Civil Engineering*, *29*(13), 2655–2671. https://doi.org/10.1080/19648189.2025.2494131.
59. Yu, W., Bu, Y., Yao, J., Zhang, S., Zhao, Y., Huang, X., & Ni, W. (2025). Leaching behavior and stabilization/solidification characterization of heavy metals from silicomanganese slag. *Journal of Hazardous Materials, 485*, Article 136915.
60. Liu, Q., Li, J., Lu, Z., Li, X., Jiang, J., Niu, Y., & Xiang, Y. (2022). Silicomanganese slag: Hydration mechanism and leaching behavior of heavy metal ions. *Construction and Building Materials, 326*, Article 126857.
61. Nasir, M., Johari, M. A. M., Maslehuddin, M., & Yusuf, M. O. (2020). Magnesium sulfate resistance of alkali/slag activated silico-manganese fume-based composites. *Construction and Building Materials, 265*, Article 120851.
62. Nasir, M., Johari, M. A. M., Yusuf, M. O., Maslehuddin, M., & Al-Harthi, M. A. (2020). Effect of alkaline activators on the fresh properties and strength of silico-manganese fume-slag activated mortar. *Advances in Concrete Construction*, *10*(5), 403-416. https://doi.org/10.12989/acc.2020.10.5.403.
63. Nasir, M., Megat Johari, M. A., Yusuf, M. O., Maslehuddin, M., Al-Harthi, M. A., & Dafalla, H. (2019). Impact of slag content and curing methods on the strength of alkaline-activated silico-manganese fume/blast furnace slag mortars. *Arabian Journal of Science and Engineering, 44*, 8325–8335.
64. Gawah, Q., Al-Osta, M. A., Maslehuddin, M., Abdullah, M. A., Shameem, M., & Al-Dulaijan, S.U. (2022). Development of sustainable self-compacting concrete utilising silico manganese fume. *European Journal of Environmental and Civil Engineering*, *27*(5), 1897–1918. https://doi.org/10.1080/19648189.2022.2102083.
65. Nasir, M., Megat Johari, M. A., Maslehuddin, M., & Yusuf, M. O. (2021). Sulfuric acid resistance of alkali/slag activated silico-manganese fume-based mortars. *Structural Concrete, 22*, Article E400–E414.
66. Amin, M. N., Murtaza, T., Shahzada, K., Khan, K., & Adil, M. (2019). Pozzolanic potential and mechanical performance of wheat straw ash incorporated sustainable concrete. *Sustain, 11*(2), Article 519. https://doi.org/10.3390/su11020519
67. Nasir, N., Adeyemi, A., Bahraq, A. A., Arif, A. M., Hasan, M. A., Mohammed, I., & Olalekan, Y. M. (2024). Strength, Microstructure, and Life Cycle Assessment of Silicomanganese Fume, Silica Fume, and Portland Cement Composites Designed Using Taguchi Method. *Journal of Materials in Civil Engineering, 36*, 4024190. https://doi.org/10.1061/JMCEE7.MTENG-17318
68. Choi, S., Kim, J., Oh, S., & Han, D. (2017). Hydro-thermal reaction according to the CaO/SiO_2 mole-ratio in silico-manganese slag. *Journal of Material Cycles and Waste Management, 19*, 374–381. https://doi.org/10.1007/s10163-015-0431-6
69. Frı´as, M., & Rodrı´guez, C. (2008). Effect of incorporating ferroalloy industry wastes as complementary cementing materials on the properties of blended cement matrices. *Cement and Concrete Composites, 30*, 212–219. https://doi.org/10.1016/j.cemconcomp.2007.05.004
70. Navarro, R., Alcocel, E. G., Sánchez, I., Garcés, P., & Zornoza, E. (2020). Corrosion resistance of steel reinforcements embedded in alkali activated ground granulated SiMn slag mortars. *Construction and Building Materials, 230*, Article 116917. https://doi.org/10.1016/j.conbuildmat.2019.116917
71. Nath, S. K., & Kumar, S. (2016). Evaluation of the suitability of ground granulated silico-manganese slag in Portland slag cement. *Construction and Building Materials, 125*, 127–134. https://doi.org/10.1016/j.conbuildmat.2016.08.025
72. Nath, S. K., & Kumar, S. (2019). Influence of granulated silico-manganese slag on compressive strength and microstructure of ambient cured alkali-activated fly ash binder. *Waste and Biomass Valorization, 10*, 2045–2055. https://doi.org/10.1007/s12649-018-0213-1
73. Nath, S. K., & Kumar, S. (2017). Reaction kinetics, microstructure and strength behavior of alkali activated silico-manganese (SiMn) slag fly ash blends. *Construction and Building Materials, 147*, 371–379. https://doi.org/10.1016/j.conbuildmat.2017.04.174
74. Kumar, S., García-Triñanes, P., Teixeira-Pinto, A., & Bao, M. (2013). Development of alkali activated cement from mechanically activated silico-manganese (SiMn) slag. *Cement and Concrete Composites, 40*, 7–13. https://doi.org/10.1016/j.cemconcomp.2013.03.026
75. Tamayo, P., del Angel, G. G., Setién, J., Soto, A., & Thomas, C. (2023). Feasibility of silicomanganese slag as cementitious material and as aggregate for concrete. *Construction and Building Materials*. https://doi.org/10.1016/j.conbuildmat.2022.129938
76. Frias, M., Sánchez De Rojas, M. I., Santamaría, J., & Rodríguez, C. (2006). Recycling of silicomanganese slag as pozzolanic material in Portland cements: Basic and engineering properties. *Cement and Concrete Research, 36*, 487–491. https://doi.org/10.1016/j.cemconres.2005.06.014
77. Allahverdi, A., & Ahmadnezhad, S. (2014). Mechanical activation of silicomanganese slag and its influence on the properties of Portland slag cement. *Powder Technology, 251*, 41–51. https://doi.org/10.1016/j.powtec.2013.10.023
78. Razzaq, W., Elkatatny, S., Gowida, A., & Samsuri, A. (2022). Application of silicomanganese fume as a novel bridging material for water-based drilling fluids. *ACS Omega*. https://doi.org/10.1021/acsomega.2c05456
79. Razzaq, W., Elkatatny, S., Gamal, H., & Samsuri, A. (2022). The utilization of steelmaking industrial waste of silicomanganese fume as filtration loss control in drilling fluid application. *Journal of Energy Resources Technology*. https://doi.org/10.1115/1.4051197
80. Najamuddin, S. K., Johari, M. A. M., Maslehuddin, M., & Yusuf, M. O. (2019). Synthesis of low temperature cured alkaline activated silicomanganese fume mortar. *Construction and Building Materials, 200*, 387–397. https://doi.org/10.1016/j.conbuildmat.2018.12.056
81. Frías, M., de Rojas, M. I. S., & Rodríguez, C. (2009). The influence of SiMn slag on chemical resistance of blended cement pastes. *Construction and Building Materials, 23*, 1472–1475. https://doi.org/10.1016/j.conbuildmat.2008.06.012
82. Criado, M., Ke, X., Provis, J. L., & Bernal, S. A. (2017). Alternative inorganic binders based on alkali-activated metallurgical slags. In H. S. Junior, J. Fiorelli and S. F. D. Santos (Eds.), *Sustainable and Nonconventional Construction Materials using Inorganic Bonded Fiber Composites* (First ed., pp. 185-220). Elsevier.
83. Alwaeli, M., Gołaszewski, J., Niesler, M., Pizoń, J., & Gołaszewska, M. (2020). Recycle option for metallurgical sludge waste as a partial replacement for natural sand in mortars containing CSA cement to save the environment and natural resources. *Journal of Hazardous Materials, 398*, Article 123101.
84. Criado, M., Bernal, S. A., Garcia-Triñanes, P., & Provis, J. L. (2018). Influence of slag composition on the stability of steel in alkali-activated cementitious materials. *Journal Of Materials Science, 53*, 5016–5035. https://doi.org/10.1007/s10853-017-1919-3
85. Frias, M., de Rojas, M. I. S., Menendez, I., de Lomas, M. G., & Rodriguez, C. (2005). Properties of SiMn slag as apozzolanic material in portland cement manufacture. *Mater. Construcción, 55*, 53–62.
86. Péra, J., Ambroise, J., & Chabannet, M. (1999). Properties of blast-furnace slags containing high amounts of manganese. *Cement and Concrete Research, 29*, 171–177. https://doi.org/10.1016/S0008-8846(98)00096-9
87. Choi, S., Kim, J., Oh, S., & Han, D. (2017). Hydro-thermal reaction according to the CaO/SiO_2 mole-ratio in silico-manganese slag. *Journal of Material Cycles and Waste Management, 19*, 374–381.
88. Cota, T. G., de M.S. Cheloni, L. M., Guedes, J. J. M., & Reis, É. L. (2023). Silico-manganese slag and its utilization into alkali-activated materials: A critical review. *Construction and Building Materials, 399*, Article 132589.
89. Navarro, R., Zornoza, E., Garcés, P., Sánchez, I., & Alcocel, E. G. (2017). Optimization of the alkali activation conditions of ground granulated SiMn slag. *Construction and Building Materials, 150*, 781–791. https://doi.org/10.1016/j.conbuildmat.2017.06.064

90. Nasir, M., Johari, M. A. M., Adesina, A., Maslehuddin, M., Yusuf, M. O., Mijarsh, M. J. A., Ibrahim, M., & Najamuddin, S. K. (2021). Evolution of room-cured alkali-activated silicomanganese fume-based green mortar designed using Taguchi method. *Construction and Building Materials, 307*, Article 124970. https://doi.org/10.1016/j.conbuildmat.2021.124970
91. Najamuddin, S. K., Johari, M. A. M., Bahraq, A. A., Yusuf, M. O., Maslehuddin, M., & Ibrahim, M. (2024). Silicomanganese fume-based alkali-activated mortar: experimental, statistical, and environmental impact studies. *Environ Sci Pollut Res*, *31*, 61525–61540. https://doi.org/10.1007/s11356-024-35325-z.
92. Nasir, M., Johari, M. A. M., Yusuf, M. O., Maslehuddin, M., & Al-Harthi, M. A. (2019). Synthesis of alkali-activated binary blended silico-manganese fume and ground blast furnace slag mortar. *Journal of Advanced Concrete Technology, 17*, 728–735.
93. Nasir, M., Johari, M. A. M., Maslehuddin, M., Yusuf, M. O., & Al-Harthi, M. A. (2020). Influence of heat curing period and temperature on the strength of silico-manganese fume-blast furnace slag-based alkali-activated mortar. *Construction and Building Materials, 251*, Article 118961.
94. Nasir, M., Johari, M. A. M., Maslehuddin, M., & Yusuf, M. O. (2021). Sodium sulfate resistance of alkali/slag activated silico–manganese fume-based composites. *Structural Concrete, 22*, Article E415–E429.
95. Concrete, S. C. (2005). The European guidelines for self-compacting concrete. *BIBM*, *22*, 563.
96. Ibrahim, M., Maslehuddin, M., Khallaf, Z. A., Joseph, J. J. I., & Mamilla, S. B. (2025). Brine sludge activated ground volcanic pumice-based alkali activated binder. *Construction and Building Materials, 483*, Article 141836.
97. Liew, Y. M., Kamarudin, H., Mustafa Al Bakri, A. M., Bnhussain, M., Luqman, M., Khairul Nizar, I., Ruzaidi, C. M., & Heah, C. Y. (2012). Optimization of solids-to-liquid and alkali activator ratios of calcined kaolin geopolymeric powder. *Construction and Building Materials, 37*, 440–451. https://doi.org/10.1016/j.conbuildmat.2012.07.075
98. Nasir, M., Megat Johari, M. A., Maslehuddin, M., & Yusuf, M. O. (2021). Sulfuric acid resistance of alkali/slag activated silico-manganese fume-based mortars. *Structural Concrete, 22*, Article E400–E414. https://doi.org/10.1002/suco.201900543
99. Al-Duais, I. N. A., Ahmad, S., Al-Osta, M. A., Maslehuddin, M., & Saleh, T. A. (2024). Properties of alkali-activated concrete made using the optimum combinations of precursor materials and activation parameters. *Journal of Materials in Civil Engineering*. https://doi.org/10.1061/jmcee7.mteng-16944
100. World Resources Institute. (2023). *State of Climate Action 2023*. https://doi.org/10.46830/wrirpt.23.00010.
101. Juenger, M. C. G., Snellings, R., & Bernal, S. A. (2019). Supplementary cementitious materials: New sources, characterization, and performance insights. *Cement and Concrete Research, 122*, 257–273. https://doi.org/10.1016/j.cemconres.2019.05.008
102. International Organization for Standardization. (2006). *Environmental management – Life cycle assessment, principles and framework* (ISO 14040). ISO.
103. Nematollahi, B., Sanjayan, J., Qiu, J., & Yang, E. H. (2017). Micromechanics-based investigation of a sustainable ambient temperature cured one-part strain hardening geopolymer composite. *Construction and Building Materials, 131*, 552–563. https://doi.org/10.1016/j.conbuildmat.2016.11.117
104. Ouellet-Plamondon, C., & Habert, G. (2015). *Life cycle assessment (LCA) of alkali-activated cements and concretes*. Woodhead Publishing Limited. https://doi.org/10.1533/9781782422884.5.663
105. Nazari A., Sanjayan Jay G. (2017). *Handbook of Low Carbon Concrete.* Kidlington.
106. Hong, T., Ji, C., & Park, H. (2012). Integrated model for assessing the cost and CO_2 emission (IMACC) for sustainable structural design in ready-mix concrete. *Journal Of Environmental Management, 103*, 1–8. https://doi.org/10.1016/j.jenvman.2012.02.034
107. Miniggio Y. M., Nærland L., Aaserud T. I. (2020). *Environmental Aspects of Utilising Silicomanganese Slag as a Cement Substitute.* University of Agder Norway.
108. Sirico, A., Bernardi, P., Belletti, B., Sciancalepore, C., Milanese, D., Paini, A., & Vignali, G. (2024). Environmental and mechanical analysis of low-carbon concrete with vitrified MSW incineration bottom ash as cement replacement. *Structural Concrete, 25*, 2968–2990.

Publisher's Note